HEAT TRANSFER THROUGH A ROTATING BALL BEARING AT LOW ANGULAR VELOCITIES

by

Sarah Isert

A report submitted in partial fulfillment
of the requirements of the degree

of

MASTER OF SCIENCE

in

Mechanical Engineering

Approved:

Dr. Stephen A. Whitmore Major Professor	Dr. Heng Ban Committee Member

Dr. Barton L. Smith
Committee Member

UTAH STATE UNIVERSITY
Logan, Utah

2011

ABSTRACT

Heat Transfer through a Rotating Ball Bearing

at Low Angular Velocities

by

Sarah Isert, Master of Science

Utah State University, 2011

Major Professor: Dr. Stephen A. Whitmore
Department: Mechanical and Aerospace Engineering

Bearings are commonly used in mechanical systems when there are rotating parts in the system. For bearings that run at speeds above about 1000 revolutions per minute, such as those used in aircraft turbines, machining tools, and automotive engines, it is important to take into account the heat transfer through the bearing system due to friction. Heat transfer is generally not considered for applications where the bearing is rotating at low speeds, such as clocks and bicycles. However, for certain aerospace applications, such as precision instruments or wind turbines, the heat transfer through the bearing becomes relevant. The case where the bearing is rotating rapidly has been extensively studied in the literature; however, bearings rotating at low speeds are not often studied due to the small amount of heat flowing through the bearing. This report extends the current body of knowledge by analytically determining the thermal resistance of bearings that rotate at low angular velocities and comparing the analytic values to experimental values. Using this information will help in system design where an accurate knowledge of bearing heat transfer is needed.

Thermal resistance is a measure of temperature drop due to the resistance of an object to heat flow. A literature review led to the conclusion that for increasing rotational speeds the thermal resistance of the bearing should decrease due to increased convection heat transfer on the inside surfaces of the bearing. Using correlations from the literature a bearing heat transfer model was developed to provide a quick engineering tool to determine the thermal resistance of a bearing given the bearing dimensions, rotational speed, and input heat flow.

A rough examination of the heat transfer model was made using an experimental apparatus developed to sense the temperature drop across a representative bearing system. This apparatus allowed the thermal resistance to be calculated and compared against predicted model values. This test was repeated for several different shaft rotational rates.

(76 pages)

This report is dedicated to those who believe in me even when I don't, and to all those who gave me chocolate and cookies as I worked on this project. You are appreciated.

ACKNOWLEDGMENTS

I would like to thank my committee members, Drs. Stephen A. Whitmore, Heng Ban, and Barton L. Smith for their support and guidance not only through this project but throughout my whole tenure at Utah State University. We students are always watching, and your examples and dedication to helping us learn have not gone unnoticed or unappreciated.

The assistance and support of the Northrop Grumman Corporation is gratefully recognized. This material is based upon work supported by the National Science Foundation Graduate Research Fellowship under Grant No. 1147384.

Sarah Isert

TABLE OF CONTENTS

Page

ABSTRACT....ii

ACKNOWLEDGMENTS....v

LIST OF TABLES....vii

LIST OF FIGURES....viii

NOMENCLATURE....ix

INTRODUCTION....1

REPORT STATEMENT....2

LITERATURE SURVEY....3

Bearings....3
Fluid Dynamics....4
Couette flow....4
Taylor-Couette flow....5
Dean flow....7
Bearing Ball Flow....8
Heat Transfer....9
Race Resistance....10
Bearing Ball Resistance....10
Couette/Taylor-Couette Flow Heat Transfer....11
Dean Flow Heat Transfer....14

OBJECTIVES....15

APPROACH....17

Model Development....17
Bearing Race Thermal Resistance....17
Bearing Ball....19
Circular Couette/Taylor-Couette Flow Resistance....20
Dean Flow Section Thermal Resistance....22
Collected Algorithm....22

EXPERIMENTAL VALIDATION....24

Experimental Apparatus....24
Experimental Procedure....32
Data Reduction and Analysis....33

RESULTS AND DISCUSSION....35

Page

Analytic vs. Experimental Comparisons 35
Uncertainty Analysis.....38

CONCLUSIONS.....44

REFERENCES.....46

APPENDICES.....50

MATLAB Driver Code.....50
Experimental Data Uncertainty.....57
Taylor Section Nusselt Number Calculation Function.....64
Dean Section Nusselt Number Calculation Function.....64

LIST OF TABLES

Page

Table 1: Race Dimensions.....18

Table 2: Bearing Lengths.....19

Table 3: Measurements and Data Acquisition.....25

Table 4: Shaft Properties.....27

Table 5: Bearing Dimensions and Properties.....28

Table 6: Analytic Correlation Properties and Uncertainties.....39

Table 7: Calculated Properties' Uncertainties.....40

Table 8: Uncertainty of Resistances.....41

Table 9: Experiment Uncertainties.....42

LIST OF FIGURES

Page

Figure 1: Bearing flow scenario description....4

Figure 2: Thermal resistance network....9

Figure 3: Bearing ball plane wall model....19

Figure 4: Experiment block diagram....24

Figure 5: Experiment setup....27

Figure 6: Bearing dimensions....29

Figure 7: Battery characterization test....31

Figure 8: Uncorrected bearing and shaft thermal resistances....35

Figure 9: Bearing thermal resistance vs. angular velocity....37

Figure 10: Convection coefficients vs. angular velocity....38

Figure 11: Uncertainty on the data....43

NOMENCLATURE

A	-	amperes
A_{ta}	-	Taylor-Couette flow heat transfer area, m^2
A_{wall}	-	bearing ball contact area, m^2
a	-	pipe diameter, m
ºC	-	degrees Celsius
d	-	Taylor-Couette gap length, m
d_{ball}	-	Bearing ball diameter, m
De	-	Dean number, unitless
g	-	acceleration due to gravity, m/s^2
Gr	-	Grashof number, unitless
h_{Ta}	-	convection coefficient for Taylor-Couette flow, W/m^2-K
J	-	joules
K	-	degrees Kelvin
k	-	thermal conductivity, W/m-K
k_{air}	-	thermal conductivity of air, W/m-K
k_{steel}	-	thermal conductivity of steel, W/m-K
L	-	length, m
m	-	meters
N	-	number of samples
n	-	exponent for Taylor-Couette flow Nusselt number, unitless
Nu_{cond}	-	Nusselt number for circular Couette flow, unitless
Nu_{De}	-	Nusselt number for Dean flow, unitless
Nu_{Ta}	-	Nusselt number for Taylor-Couette flow, unitless
P	-	power, W
Pr	-	Prandtl number, unitless
q	-	power, W
R	-	electrical resistance, ohms
r	-	generic radius, m
R_1	-	inner radius of a cylinder, m
R_2	-	outer radius of a cylinder, m
rad	-	radians
Re	-	Reynolds number, unitless
Re_{crit}	-	critical Reynolds number, unitless
R_i	-	inner Taylor cylinder radius, m
RIRI	-	inner race inner radius, m
RIRO	-	inner race outer radius, m
RIRW	-	inner race raceway radius, m
RORI	-	outer race inner radius, m
RORO	-	outer race outer radius, m
RORW	-	outer race raceway radius, m
R_m	-	mean raceway radius, m
rpm	-	revolutions per minute
R_{th}	-	thermal resistance, K/W
$R_{th,Ta}$	-	thermal resistance of Taylor-Couette section, K/W
$R_{th,conv}$	-	thermal resistance due to convection, K/W
$R_{th,ball}$	-	thermal resistance of bearing ball, K/W
s	-	seconds
Ta	-	Taylor number, unitless

Ta_c	-	critical Taylor number, unitless
u_c	-	centerline velocity, m/s
u_θ	-	velocity between cylinders, m/s
V	-	volts
W	-	watts
x_1	-	Parameter for Dean flow Nusselt number, unitless
x_2	-	Parameter for Dean flow Nusselt number, unitless
ΔT	-	Change in temperature, ºC
Ω	-	ohms
α	-	thermal diffusivity, m/s^2
β	-	Coefficient of volumetric thermal expansion, 1/K
σ	-	rotational parameter, unitless
σ_x	-	standard deviation
ω	-	angular velocity, rad/s, rev/s, rpm
υ	-	kinematic viscosity, m^2/s

INTRODUCTION

Rotating machinery is commonly used in mechanical applications, and ball bearings are often used to support the rotating mechanisms. Heat transfer through systems that include ball bearings has been studied, particularly for applications that include very high angular velocities such as spindles on machining tools or bearings in aircraft engines. However, the literature has little information with regard to bearing heat transfer at low ($\omega < 1000$ rad/s) angular velocities.

To gain a theoretical background the fluid mechanics of the problem were studied to determine the flow regimes inside the bearing. The bearing is modeled as a combination of two different flow regimes: circular Couette/Taylor-Couette flow and Dean flow [1,2]. The resistance due to these convection conditions and the bearing races and the bearing balls were studied and considered.

The bearing thermal resistance was coded using the MATLAB programming language. To test the code, a simple experiment was designed to measure the thermal resistance of a standard, off-the-shelf deep groove angular contact ball bearing. Data was taken over a range of angular velocities, focusing on the region between 300 and 500 rpm due to the interest in low angular velocities. The convection coefficient and thermal resistance were calculated and compared. An uncertainty model was developed from the experimental data and will be presented later in the Results and Discussion – Uncertainty Analysis section. Conclusions from the experiment are discussed, as are suggestions for future experiments of these types.

REPORT STATEMENT

This report proposes to investigate the values of thermal resistance and heat transfer coefficients for ball bearings with Reynolds numbers lower than 350 in both the Dean and Taylor-Couette flow. The thermal resistance will be calculated analytically and compared to experimental results. The thermal resistance is expected to be constant for speeds below a critical Taylor number then decrease steadily thereafter. The end product will be a simple program to calculate the thermal resistance that takes into account bearing dimensions, bearing ball thermal resistance, and convection coefficients.

LITERATURE SURVEY

Before beginning this project a literature survey was conducted for subject matter relevant to heat transfer through bearings. Much of the current research is on bearings in extreme environments that rotate at high angular velocities. These bearing applications are unlike the bearing conditions under consideration for this project – that is, bearings that rotate at low angular velocities in benign environments. The research was divided into three major topics: general research on heat transfer through bearings, fluid dynamics, and heat transfer specific to the flow conditions and geometry through the bearings. The results of the literature survey are described below, and the major findings are discussed further in the Approach – Model Development section.

Bearings

The heat transfer through bearings has been extensively studied. Though most bearings operate in environments where the heat generation rate is low and/or the ability to remove heat from the bearing is sufficient, some applications operate in adverse environments [3]. Present research focuses on bearings that operate at high speeds in extreme environments, such as those found in aircraft turbine engines [4] and in high-speed machining spindles [5]. Depending on the application, these bearings can operate at high speeds, usually between 10,000 and 25,000 rpm. Instead of being studied on the component level these bearings are often studied as the total assembly mechanism due to the high heat load on the bearings,.

Though the literature contains a wealth of information on high-speed bearing assemblies, information on individual bearings at angular velocities less than $\omega < 1000$ rpm is not readily available, particularly as it relates to heat transfer. Low-speed bearings have applications in precision instruments, and the heat transfer through the bearings can be important.

Fluid Dynamics

The fluid in the bearing under study is modeled as shown in Fig. 1 with two flow scenarios, Couette flow transitioning to Taylor-Couette flow and Dean flow. Discussion of these flows and rationale for their uses is presented below. A further discussion of fluid mechanics as pertains to the perturbing effect of the bearing balls, retainer, and other perturbation sources is also included below.

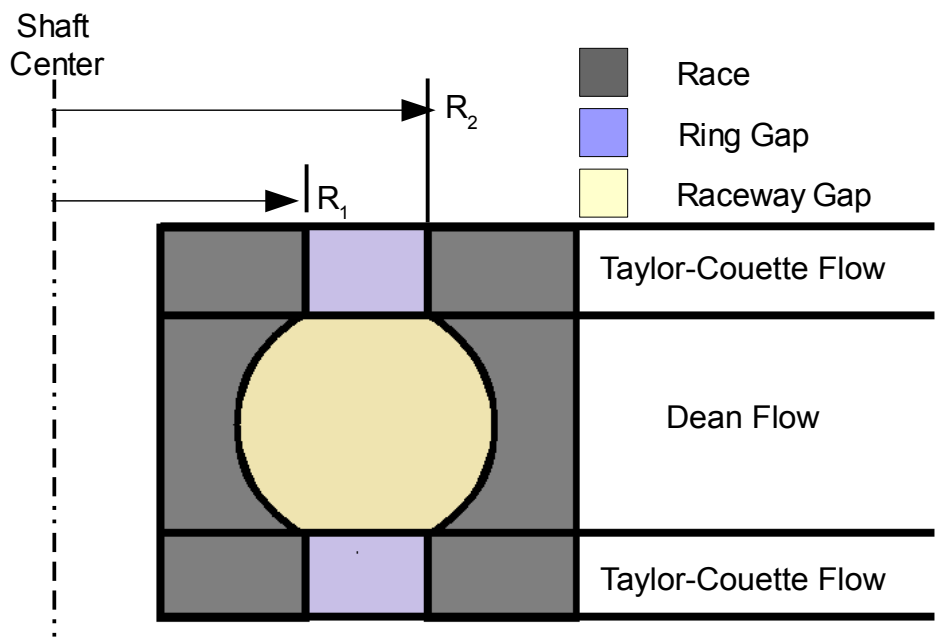

Figure 1: Bearing flow scenario description.

<u>Couette flow</u>

Couette flow is defined generally as flow between two plates produced by relative motion of the plates. The flow is driven purely by the relative motion of the plates, and not by a pressure gradient as is found in Couette-Poiseuille flow [6]. When the flow takes place between two concentric cylinders it is known as circular Couette flow.

Reynolds numbers for Couette flow are typically calculated using the center line velocity u_c [7]. For plane Couette flow, since the velocity profile is linear, this is calculated by dividing the moving plate velocity in half. In the case of closely spaced concentric cylinders in which one cylinder is fixed and the other rotates with a constant angular velocity the velocity profile between two cylinders can be approximated as linear. The linear velocity profile holds for situations where, based off the radius of the inner cylinder R_1 and the radius of the outer cylinder R_2 [8]

$$R_2 - R_1 \ll R_1 \tag{1}$$

However, this situation is not valid for ball bearings in general as they have a relatively large gap between the races. Therefore, a large gap approximation must be made. For circular Couette flow with a large gap between the cylinders the velocity profile is not linear. It can be calculated by [9]

$$u_\theta = \frac{1}{(1-(R_1/R_2)^2)}\left\{\left[-\omega\left(\frac{R_1}{R_2}\right)^2\right]r + \frac{R_1^2}{r}\omega\right\} \tag{2}$$

Here u_θ is the linear fluid velocity in the cylinder gap at a specific radius, r is the radius the velocity is being calculated at, and ω is the angular velocity of the inner cylinder. Note that the equation in this form is only valid for a rotating inner cylinder and a stationary outer cylinder.

Taylor-Couette flow

Flow between two concentric cylinders does not stay stable under all conditions. After a certain point defined by the fluid's viscosity, cylinder rotational speed, and cylinder gap length the fluid will begin to develop vortices known as Taylor vortices. This point is found via the Taylor number (*Ta*), which can be calculated from [10]

$$Ta = \frac{R_1 d^3 \omega}{\nu^2} \tag{3}$$

Here R_1 is the inner cylinder radius, d is the gap length between the inner and outer cylinder, ω is the angular velocity of the inner cylinder, and υ is the kinematic viscosity.

Fluid buoyancy can also be an important contributor to flow between the bearing races. The more significant fluid buoyancy becomes, the more the flow deviates from the ideal Taylor-Couette approximation. As the fluid buoyancy becomes very high, the flow properties begin to resemble natural convection. The significance of fluid buoyancy is determined by the non-dimensional rotational parameter [11]

$$\sigma = Gr / Re^2 \tag{4}$$

In this case, since *Gr,* the Grashof number, is small compared to the square of the Reynolds number *Re*, the rotational effects dominate over the buoyancy effects. The rotational parameter σ is never greater than about 0.002, so the flow therefore approaches the isothermal, Taylor-Couette situation [11].

Viscosity has a stabilizing effect in Couette flows. Rayleigh's circulation criterion states that for an inviscid stable flow the following condition applies [12]:

$$\omega_2 > \left(\frac{R_1}{R_2}\right)^2 \omega_1 \tag{5}$$

In this equation ω1 is the rotational velocity of the inner cylinder and ω2 is the rotational velocity of the outer cylinder. From Eq. 5, known as the Rayleigh line, it can be seen that when the inner cylinder is rotated and the outer cylinder is stationary, such as for the case in this study, the flow is unstable. However, viscosity stabilizes the flow up to a certain speed. This speed can be found from the Taylor number (Eq. 3).

If the Taylor number is above a critical value of about $Ta_c \approx 1708$ (for a rotating inner cylinder only) [12] the flow becomes three-dimensional with a series of stacked spiral vortices. If

the velocity becomes sufficiently high, the Taylor cells gain a wavy structure. If the Taylor number is very high the vortices become turbulent [12]. There are many stability boundaries, and when the outer cylinder is rotated as well as the inner cylinder many different flow regimes and vortices can be produced.

For rotating flows between two cylinders a negative temperature gradient (heated inner cylinder and cooled outer cylinder) is stabilizing [10]. This effect tends to counter the instability properties described in the previous paragraph and delay the transition to turbulence or damp instabilities cause by fluidic disturbances.

Dean flow

Dean flow occurs in curved channels where the radius of curvature is much larger than the channel width. The flow differs from Couette flow and Taylor-Couette flow as the curvature of the channel causes a secondary flow to form. This secondary flow can significantly increase the heat transfer rate [13]. Dean flow can be characterized by the Dean number (*De*), defined as

$$De = Re\left[\frac{d}{2\,R_m}\right]^{1/2} \tag{6}$$

In Eq. 6 *Re* is the Reynolds number, d is the diameter of the raceway, and R_m is the mean raceway radius. Normally Dean flow is considered to be pressure driven, much like Poiseuelle flow. Applying Rayleigh's criterion (Eq. 5) to the pressure driven scenario produces stable flow along the inside surface of the channel and unstable flow along the outside surface of the channel [12]. In the case under study, however, the Dean flow is driven by the rotation of the inner cylinder. Driving the flow by rotation rather than by a pressure difference causes the flow to behave much like the circular Couette flow above and, according to Rayleigh's criterion, the flow is unstable over all radii. This instability results in the formation of a secondary flow.

However, as with Taylor flow, the viscosity has a stabilizing role in the flow. Dean flow is

laminar until a critical Reynolds number (Re_{crit}) is exceeded. This number is based on the mean gap radius and the gap length and can be found from [14]

$$Re_{crit} = 2100\left(1 + \frac{12}{\sqrt{\frac{R_m}{d}}}\right) \tag{7}$$

Exceeding the critical Dean number results in the development of a secondary stable laminar flow pattern with a vortex or vortices superimposed on the main flow [12]. These vortices form in addition to the corner vortices that exist naturally [15]. Note that non-negligible effects due to curvature exist even at very low Reynolds numbers, and are very different from effects produced at high Reynolds numbers [16].

Dean flow occurs in curved channels, such as in helical coils, and is usually driven by a pressure gradient. The bearing raceway is modeled as a helical coil with a 0° pitch angle, but unlike a helical coil the raceway is not closed at the top and bottom. For a general bearing, there may be fluid transfer between the Couette and Dean sections of the bearing. However, it is interesting to note that experimental data show that Taylor vortices do not move axially once they set up [11]. In some cases this effect may help slow or inhibit fluid flow between sections.

When a curved pipe rotates about the axis normal to the plane that includes the pipe, the Coriolis force can also contribute to the generation of secondary flow [14]. The fluid flow and heat transfer are different between the rotating and the stationary case, and solutions for one will not apply to the other. However, when the rotation is positive, that is, in the same direction as fluid flow, the flow structure is similar to that of stationary flow [15].

Bearing Ball Flow

Modeling the bearing as a combination of Couette/Taylor-Couette and Dean flow scenarios is complicated by the presence of the bearing balls in the raceway. The balls act as a

branch of the heat flow path, but they also act as a perturbation source for the flow. The flow around the bearing balls themselves must be considered in the analysis to determine what effect the perturbation will have on the general flow field.

Kreith et al. studied the fluid dynamics of a rotating sphere in an infinite medium [18]. The result of their experiments was that below $Re = 5 \cdot 10^5$ the flow around the sphere was mostly laminar, but with a turbulent separation zone near the equator. Note that the equator is defined as the diameter perpendicular to the axis of rotation. In a ball bearing, as the balls rotate the equator of the bearing will be continually changing – there will not be one circumference of the bearing that will remain as the equator. In addition to this, the fluid in the raceway is not an infinite medium, and the separating fluid will interact with the walls of the bearing. The separating fluid could be enough of a perturbation source to cause the flow in the raceway to be turbulent.

Heat Transfer

Figure 2 shows the bearing thermal resistance network. There are two types of resistances in the circuit, those due to the structure and those due to convection. The structural resistances can be broken down further to the resistances due to the inner race, outer race, and bearing balls. The convection resistances are caused by fluid movement due to the spin of the bearing on the shaft. The resistances will be discussed in further detail in the following sections.

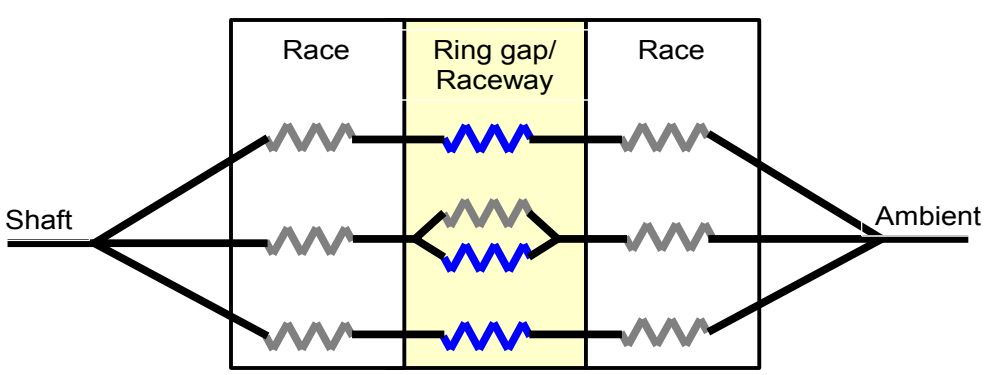

Figure 2: Thermal resistance network.

Race Resistance

The thermal resistance (R_{th}) of the bearing races was found using the cylindrical thermal resistance formula found in [19]

$$R_{th} = \frac{\ln(R_2/R_1)}{2\pi L k} \tag{8}$$

Here R_1 and R_2 are the inner and outer radii of the section under consideration, respectively, L is the length of the section under consideration, and k is the thermal conductivity of the material. The thermal resistance of the race will not change as the angular velocity of the shaft changes.

There will be some change in the bearing dimensions due to the temperature change across the bearing. However, the coefficient of thermal expansion is small – 11.9 μm/m-ºC between 23 and 280 ºC [18].As the temperature change does not exceed 10°C the percent length change over the length is on the order of 0.01%. For this analysis dimensional changes due to thermal expansion were assumed to be negligible. Note that this will not be the case for all bearings, particularly those with large temperature changes across the bearing or those with a higher coefficient of thermal expansion.

Bearing Ball Resistance

The bearing balls are an important heat flow path in the bearing and their conduction resistance has been extensively studied. Mizuta et al. [21] thoroughly studied the thermal conductance of the bearing balls and their effect on heat transfer. This study examined bearings rotating at speeds between 600 rpm and 4,000 rpm. They concluded that the bearing balls are the dominant heat carrier under an oil lubrication condition.

Yovanovich in [22] and Bairi et al. in [23] concluded that bearing ball thermal resistance depends on axial force, bearing preload, thermal expansion effects, material properties, and

contact patch area. Also important are boundary conditions on the bearing ball, such as whether it is in a vacuum, lubricated, or in air, and whether or not the contact is considered to be perfect.

A major assumption of Bairi et al. is that all the heat generated by frictional heating or a generalized heat flux is transferred out entirely by the bearing ball surface [23]. This approach is useful, as it simplifies the governing equations, but it does not apply to the case being studied, where there is a net heat flux from the shaft to the outer race due to the temperature difference between the shaft and outer race. The results of the analytical model indicate that convection alone is not enough to account for the heat transferred through the bearing, and the bearing balls must play a part in the heat transfer. Therefore, there must be a net heat flux through the bearing ball which requires that not all of the heat be transferred out by the bearing ball surface.

Couette/Taylor-Couette Flow Heat Transfer

As shown in Figure 2, the convection heat transfer can be divided into two components, that in the raceway and that in the ring gaps. The heat transfer through the ring gaps is modeled as circular Couette/Taylor-Couette flow. There has been a great deal of work done on heat transfer in the Taylor-Couette flow section of the bearing, much of which deals with the scenario found in this report (see [10, 24]). Since there are many applications that deal with a heated rotating inner cylinder and a cooler stationary outer cylinder, a large portion of the body of literature dealing with Taylor-Couette flows is applicable to this report.

Generally speaking, there are two different heat transfer regimes in the fluid, conduction and convection [24]. The heat transfer regime depends on the Taylor number (Eq. 3). A dimensionless parameter called the Nusselt number (Nu) that depends on the convection coefficient h, thermal conductivity k, and a length scale L is commonly used in convection heat transfer. This number is defined as follows [19].

$$Nu = \frac{h\,L}{k} \tag{9}$$

Nusselt number correlations can be found from experiments, and the convection coefficient can be calculated from the definition of the Nusselt number and used to find the convection thermal resistance.

Before the flow transitions to turbulence, that is, during circular Couette flow, the Nusselt number is constant and can be approximated by [10]

$$Nu_{cond} = \frac{\frac{2\,d}{R_i}}{\ln\left(\frac{d}{R_i}+1\right)} \tag{10}$$

where the subscript *cond* indicates that this is the Nusselt number for the conduction regime, d is the gap length between the cylinders, and R_i is the radius of the inner cylinder [10]. Note that this number is defined differently in different references; the factor of 2 in the denominator is not present in [25]. The Couette Nusselt number correlation in Eq. 10 was used as it comes from the same reference as the Taylor-Couette Nusselt number correlation. For conduction heat transfer the Nusselt number correlation depends only on geometry, while for convection heat transfer many other parameters, such as the Taylor number, Prandtl number, and Reynolds number, come into play. Conduction heat transfer ends once a critical Taylor number is reached

Taylor vortices begin to form above a critical Taylor number. The critical Taylor number is generally taken to be $Ta_c \approx 1708$ [12]. The Nusselt number begins to increase monotonically at this point. The Nusselt number correlation for laminar Taylor-Couette flow is [10]

$$Nu_{Ta} = Nu_{cond}\left(\frac{Ta}{1708}\right)^{n/2} \tag{9}$$

where

$$n = (Pr/Gr)^{1/6} \tag{9a}$$

Here the Nusselt number for the Taylor section (Nu_{Ta}) is a function of the Nusselt number for the conduction section, the Taylor number, and an exponent that is a function of the Grashof number Gr and the Prandtl number Pr. This correlation is valid for $10^{-7} < Pr/Gr < 40$ and $Ta < 1.7 \cdot 10^{7}$.

It can be seen that the Prandl and Grashof numbers are important parameters in the Nuselt number correlations. The Grashof number is defined as [19]

$$Gr = \frac{g \beta \Delta T L^3}{\nu^2} \tag{10}$$

This number characterizes convection type (natural vs. forced) and is the ratio of buoyant to viscous forces. As can be seen it depends on gravity (g), the coefficient of thermal expansion (β), temperature difference (ΔT), a length scale (L), and kinematic viscosity (υ). Property values were taken at the mean temperature of the flow, which was defined as the average of the shaft and outer race temperatures.

The Prandtl number is [19]

$$Pr = \frac{\nu}{\alpha} \tag{11}$$

or the ratio of the momentum and thermal diffusivities in the form of the kinematic viscosity υ and the thermal diffusivity α. This number is a measure of the relative effectiveness of momentum and energy transport in the momentum and thermal boundary layers. For air, as $Pr \approx 0.7$, the energy and momentum transports are comparable, though the energy transport in the thermal boundary layer is slightly more effective. The Prandtl number strongly affects the relative growth of the thermal and momentum boundary layers.

Dean Flow Heat Transfer

Due to the axial curvature of the raceway, circular Couette/Taylor-Couette flow heat transfer was not deemed an appropriate heat transfer model for the raceways. Instead, after extensive research, Dean flow was chosen to model the raceway flow.

Vortices in a curved pipe form due to the curvature of the pipe. Above a critical Dean number another set of vortices forms, further increasing the heat transfer. It is important to note that the formation of more vortices do not indicate that the flow has transitioned to turbulence; as with Taylor-Couette flow, the flow can be vortical due to instabilities while still being laminar [16].

As stated in the Fluid Dynamics section above, heat transfer in coiled tubes can be significantly increased by the presence of secondary flow [13]. In pure Dean flow this secondary flow is caused by the curvature of the tube itself, while in rotating Dean flow an additional secondary flow can be caused by the Coriolis force [17].

For this model Nusselt numbers are calculated using the empirical correlation [14]

$$Nu_{De} = \left[\left(3.657 + \frac{4.343}{x_1} \right)^3 + 1.158 \left(\frac{De}{x_2} \right)^{3/2} \right]^{1/3} \tag{12}$$

where

$$x_1 = \left(1.0 + \frac{957}{De^2 Pr} \right)^2$$

and

$$x_2 = 1.0 + \frac{0.477}{Pr}$$

It should be noted that this correlation is for a duct with uniform temperature walls. More on this subject will be discussed in the Approach section of the report.

Other Nusselt number correlations have been proposed, such as an asypmtotic Nusselt number in [16]; however, this correlation was not applicable to the Prandtl number in this study.

OBJECTIVES

The purpose of this project is to see how the thermal resistance of a bearing changes over an angular velocity range. The thermal resistances at different angular velocities are then compared to a computer model to see how a proposed thermal resistance correlation compares to the measured thermal resistance. The desired output is a simple model for bearing thermal resistances at low Reynolds numbers. After the literature review, the project was broken down into the following tasks.

- Write a MATLAB program to predict thermal resistance for a single-row ball bearing. The code should:
  - Account for variation of properties (thermal conductivity, viscosity, etc.) with temperature if possible.
  - Take into account different flow regimes (Couette, Taylor-Couette, Dean).
  - Ensure correlations are accurate over the Reynolds/Dean numbers being tested.
  - Calculate and plot thermal resistance versus angular velocity, Reynolds number, and Taylor number.
- Build an experimental test apparatus that allows for testing of a ball bearing to validate the code. Test apparatus should
  - Include a motor system that allows testing at the desired Reynolds numbers (less than $Re = 350$ and $\omega = 1000$ rpm).
  - Provide an input heat flow via a heated shaft.
  - Enable measurements of the shaft temperature and the outer race temperature while the shaft is rotating.

  - Allow for a wide variety of input voltages and currents to the motor.
  - Provide power to the shaft heater while the shaft is rotating.
- Run several tests of the bearing at different shaft angular velocities to determine the thermal resistance. Tests should
  - Be conducted over the range of Reynolds numbers of interest.
  - Include tests run at 0 rad/s for comparison purposes.
  - Have data recorded over heat up, motor on, and cool down experiment phases to see if there are any interesting phenomena.
- Perform an uncertainty analysis on the results.
- Compare test results to MATLAB model. Discuss the results.
- Discuss follow-on tests.
- Discuss any changes made to the MATLAB model as a result of this experiment.

APPROACH

After the project was broken down as described in the Objectives section work began on the various parts of the experiment. The computer model and the experiment were developed almost simultaneously. The approaches taken are described in detail below. Briefly, for the computer model, the bearing was broken down into its component parts – races, bearing balls, and fill fluid – and the thermal resistance was calculated for each component. These thermal resistances were then summed together to find an overall thermal resistance. These calculations were performed for several angular velocities and the results plotted. For the experiment, the apparatus was constructed so the shaft was heated and the temperatures of the inner and outer races were recorded while the bearing was spinning so the steady state temperatures – and, therefore, thermal resistances – could be calculated.

Model Development

One of the purposes of this project was to create a MATLAB code to allow for a first-order approximation of the bearing thermal resistance. The code takes input bearing properties and dimensions, calculates the thermal resistance due to the bearing balls, Taylor-Couette race gap flow, and Dean raceway flow, and adds the resistances together. This is done over an angular velocity range and the results are plotted.

The following sections describe how the thermal resistance due to the bearing raceways, bearing balls, Couette/Taylor-Couette flow and Dean flow were calculated. Note that all fluid properties were taken at the mean temperature of the fluid as was done by Kreith in [10].

Bearing Race Thermal Resistance

Bearing race thermal resistance was calculated using the cylindrical thermal resistance formula described in Eq. 8. The resistance was calculated separately for the inner and outer races.

The dimensions used are found in Table 1. The inner and outer race dimensions were taken from materials provided by the manufacturer.

Table 1: Race Dimensions

	R_1 (mm)	R_2 (mm)
Inner Race	6.00	11.60
Outer Race	17.90	20.10
Inner Raceway	6.00	11.58
Outer Raceway	17.92	20.10

The raceway dimension was calculated by calculating the race gap, subtracting it from the bearing ball diameter, dividing the remainder by two, and adding and subtracting the final amount from the outer race inner radius and the inner race outer radius, respectively. It was assumed that the entire raceway section of the races are at the same thickness as the deepest point of the raceway. The thermal resistance calculated by this method will be lower than the actual thermal resistance. A more conservative approach would be to keep the raceway thickness the same as the rest of the race or to multiply the raceway thickness by a a scaling factor to account for the changing geometry due to the raceway curvature.

The thermal conductivity *k* for AISI 52100 steel, taken from [22], is 46.6 W/m-K and is valid from 20-200ºC. As the temperature range of the experiment is from 20-50ºC and no property variation with temperature data were found, the thermal conductivity was assumed to be constant. The bearing length is 0.0119. This length was divided into three sections to account for the raceway being a different thickness than the rest of the race. These lengths are shown in Table 2 .Note that the upper and lower lengths are the same as the bearing is assumed to be symmetric.

Table 2: Bearing Lengths

	Upper	Raceway	Lower
Length (mm)	3.0	5.9	3.0

As the thermal conductivity is assumed to be constant, the thermal resistance will not change with angular velocity. The bearing dimensions may change slightly with temperature as well, due to thermal expansion, but as stated above in the Literature Survey – Race Resistance section the length change is on the order of 0.01% due to the small temperature change.

Bearing Ball

The bearing ball poses a unique modeling problem. As discussed in the literature survey, the common assumption that the heat generated by frictional heating or a general heat flux is evacuated through the surface of the bearing ball as described in [23] is not valid. The bearing balls were therefore modeled as a plane wall as shown in Figure 3. The size of the contact patches in Figure 3 is greatly exaggerated.

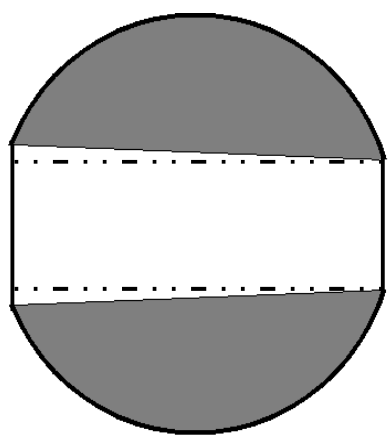

Figure 3: Bearing ball plane wall model.

The heat transfer area of the plane wall is calculated from the contact patch area, which depends on the curvature of the bearing balls, curvature of the raceway, the load on the bearing, and the material of the bearing balls and races (AISI 52100 in this case).

Once the contact patch size is calculated the thermal resistance of the bearing ball can be calculated from [19]

$$R_{th} = \frac{d_{ball}}{k_{steel} A_{wall}} \tag{13}$$

Here d_{ball} is the diameter of the bearing ball, k_{steel} is the thermal conductivity of the steel, and A_{wall} is the wall heat transfer area. Note that the contact patch area will be different at the inner and outer raceways due to the radii of curvature differing between raceways. For simplicity, the heat transfer area was taken to be the smaller (inner race) contact patch area. The contact patches differ in area by about 2.5%, so this was deemed to be a reasonable assumption.

All the heat flow into the bearing is assumed to flow out through the other side of the bearing; that is, there is no convection off the ball. The bearing will eventually reach a quasi steady state temperature distribution. As the bearing ball rotates, it will pick up heat from the inner race and transfer it to the outer race. The temperature distribution in the bearing ball is uniform; however, the rotation of the bearing ball will cause the temperature of any one point on the bearing ball to change with time. The combination of a transient bearing ball temperature and a steady-state bearing ball temperature profile complicates the heat transfer model; however, it is assumed that the heat transferred out of the “hot” side of the cycle is equal to the heat transferred into the bearing on the “cold” side of the cycle.

Circular Couette/Taylor-Couette Flow Resistance

Circular Couette/Taylor-Couette flow happens in the upper and lower sections of the bearing (see Fig. 3). The flow takes place between two cylinders, the innermost of which is

rotating. The heat transfer mode depends on the Taylor number. Over a critical Taylor number the flow transitions from circular Couette flow to laminar Taylor-Couette flow with stable vortices. The presence of the vortices increases heat transfer. Before transition to Taylor-Couette flow the Nusselt number for circular Couette flow is constant; that is, it is based solely on geometry – specifically, the gap length between the bearing races and the outer radius of the inner race (Eq. 8).

For Taylor-Couette flow the Nusselt number begins to change with Taylor number. As the shaft angular velocity increases the Taylor number increases, which in turn causes the Nusselt number to increase monotonically. Eq. 9 models this effect.

Once the Nusselt number is calculated, the Taylor-Couette section convection coefficient h_{Ta} was calculated from [19]

$$h_{Ta} = \frac{Nu_{Ta}\, d}{k_{air}} \tag{14}$$

Here d is the gap between the races and k_{air} is the thermal conductivity of air at the mean temperature. After calculating the convection coefficient the Taylor-Couette section thermal resistance $R_{th,Ta}$ is calculated using Eq. 15 found from [19]

$$R_{th,Ta} = \frac{1}{h_{Ta}\, A_{Ta}} \tag{15}$$

The surface area A_{Ta} was somewhat tricky to determine. This problem is different from many common convection problems as the heat transfers off one surface and onto another, resulting in two thermal resistances due to convection: one as the heat transfers off the inner race and one as the heat transfers into the outer race. Since h_{Ta} is assumed to be constant due to the common length scale (the race gap distance d as found in [10]) it can be pulled out of the equation and the area defined as

$$A_{Ta} = 2\pi L(R_2 + R_1) \tag{15a}$$

In this equation R_2 is the outer cylinder radius and R_1 is the inner cylinder radius. L is the length of the Taylor-Couette section.

Dean Flow Section Thermal Resistance

The Dean flow thermal resistance was calculated in a manner similar to the Couette/Taylor-Couette flow thermal resistance. The Nusselt number correlations found in Eq. 10 are used to calculate the Nusselt number. This correlation is strictly applicable for a duct with a uniform constant wall temperature. For the case being modeled there is a small but uniform temperature differential across the inner and outer bearing races. Thus radial heat flow will exist. This unmodeled effect will lead to small but consistent errors in the final results.

Collected Algorithm

Once the thermal resistances were calculated the resistances were summed in series. For the Taylor-Couette sections calculating the section thermal resistance ($R_{th,Ta}$) involved adding the inner and outer race resistances and the convection resistance. The Dean section race resistances were summed in series with the parallel summation of the Dean convection resistance and the bearing ball resistance to obtain the total Dean thermal resistance, $R_{th,De}$. The functions for the Taylor-Couette and Dean section thermal resistances are given in Eqs. 16 and 17, respectively.

$$R_{th,Ta} = R_{th,inner\,race} + R_{th,conv} + R_{th,outer\,race} \tag{16}$$

$$R_{th,De} = R_{th,inner\,race} + \frac{1}{\frac{1}{R_{th,conv}} + \frac{1}{R_{th,ball}}} + R_{th,outer\,race} \tag{17}$$

The total resistances of the three sections – two Taylor-Couette and one Dean – were then summed in parallel to find the total bearing thermal resistance as a function of angular velocity.

EXPERIMENTAL VALIDATION

This section describes the experiment setup, procedures, and how the final values were calculated. The equipment used is described here. An uncertainty analysis will be described in the Results and Discussion section. The purpose of this experiment was to determine the thermal resistance of a bearing at various angular velocities then compare this thermal resistance to those calculated in the MATLAB program. Because of the limited financial resources available to support this experiment, only a single bearing was tested. The author recognizes that a thorough evaluation of this model would require a significantly larger ensemble of bearings to be tested.

Experimental Apparatus

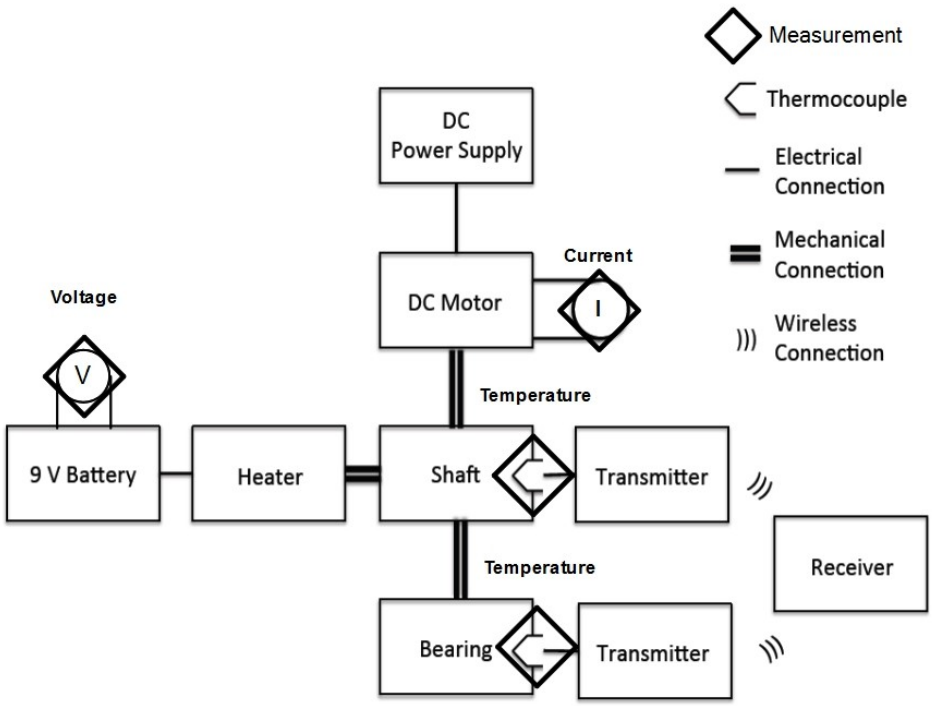

Figure 4: Experiment block diagram.

Figure 4 shows the experiment block diagram. The block diagram shows the connection types between the pieces of equipment and the locations of the sensors that were used to collect the measurements. Table 3 lists the sensors used to collect these measurements.

Table 3: Measurements and Data Acquisition

Measurement	**Sensor**	**Manufacturer**	**Specifications**	**Data Acquisition Method**
Shaft Temperature	Type K thermocouple SC-GG-K-30-36	Omega	-100-1260°C, ±0.5% of reading or 1.0°C, whichever is greater, 1.0°C temperature resolution	Wireless transmitter/Omega supplied software
Outer Race Temperature	Type K thermocouple SC-GG-K-30-36	Omega	-100-1260°C, ±0.5% of reading or 1.0°C, whichever is greater, 1.0°C temperature resolution	Wireless transmitter/Omega supplied software
Battery Voltage	Voltmeter 61-310	Ideal	0-20 V, ±(0.5% reading + 0.02) V, 3 ½ digit LED display	Manual transcription
Shaft Angular Velocity	Digital Video Camera	Canon	30 frames per second in video mode	Recorded in camera memory
Motor Current	Ammeter	B&K Precision	0-10 A, 0.5% + 2 counts accuracy, Auto-range 3 ½ digit LED display	Manual transcription

The DC motor is run by the DC power supply under constant current conditions to ensure constant angular velocity. The current to the motor was monitored and recorded.

The shaft heater is powered by a 9V battery. The battery voltage was measured at the beginning and end of each test run.

One Type K thermocouple was placed on the shaft just above the bearing and another on the outer race of the bearing. For simplicity and cost, wireless thermocouple transmitters were

used on both the shaft and the outer race.

Shaft angular velocity was measured by filming the shaft rotation on a camera, playing the video back frame by frame, and counting the number of revolutions in a period of time (usually 20 seconds). That number was converted to revolutions per minute. At slower speeds this technique was accurate to within one quarter of a revolution, but faster speeds reduced the accuracy to half a revolution. An uncertainty of ½ revolution will be used in the uncertainty analysis to be presented later in this report.

Figure 5 shows a detailed diagram of the experiment setup. The experiment support is made of wood and was designed, sized, and built specifically for this experiment. The bottom bearing plate is permanently attached to the bulk of the structure, but the top bearing plate is removable to allow access to the bearing and outer race thermocouple. Care was taken during design to ensure the bolts that attach the top bearing plate do not interfere with the shaft insulation while the system is spinning. Another consideration was making sure the inner race rotation was not hampered by the bearing plates. Sufficient inner race clearance was ensured by cutting the shaft gap diameter larger than the inner race outer diameter.

The shaft is made of Type K 3/8 inch copper tubing with properties as listed in Table 4. Diameters were found from [25] and checked by measurements in the lab. Properties were found in [26].

Copper tubing was chosen for the shaft due to its high thermal conductivity and low specific heat capacity. These properties were important as we wanted the temperature change across the shaft to be as small as possible. A small temperature drop across the shaft allows the heater to operate at a lower temperature and, more importantly for this study due to the constraint of the rotating shaft, a lower voltage.

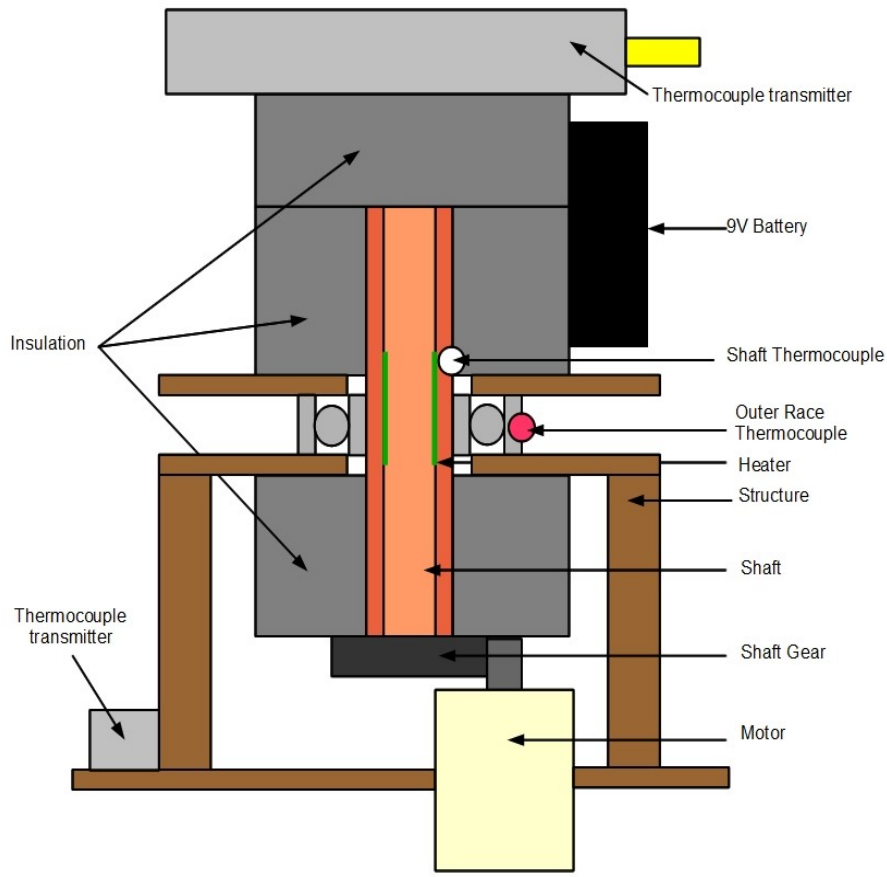

Figure 5: Experiment setup.

Table 4: Shaft Properties

Inner Diameter, m (in)	0.0102 (0.402)
Outer Diameter, m (in)	0.0127 (0.500)
Length, m (in)	0.1016 (4.0)
Thermal Conductivity, W/m-K	385 (27°C)
Specific Heat Capacity, J/kg-°C	385
Coefficient of Thermal Expansion, μm/m-°C	16.4 (25-100°C)

However, the shaft also transferred heat well along its length. Insulation was used to mitigate the longitudinal heat conduction as much as possible. One end of the shaft was connected by an end cap to the shaft gear. Temperature measurements showed this to be a significant heat flow path that caused about 60% of the heat to flow out through the gear. In retrospect this could have been at least partially prevented by using a PVC end cap instead of a copper one. The temperature drop across the bearing is lower than it could have been if the longitudinal conduction path had not been present. The lower temperature drop contributes to a greater overall uncertainty in the experimental bearing thermal resistance.

The bearing is an NSK 6203 VV shielded single row deep groove angular contact ball bearing. It is made of AISI 52100 steel. There are eight bearing balls and a cage-type bearing retainer. Bearing dimensions and other properties are given in Table 5. The properties were found from [20], and the dimensions were taken from a solid model provided by NSK. See Figure 6 for a diagram relating the dimensions to their positions on the bearing.

Table 5: Bearing Dimensions and Properties

Radius	**Figure Designation**	**Dimensions (mm)**
Inner race inner radius	RIRI	6.0000
Inner race raceway radius	RIRW	11.575
Inner race outer radius	RIRO	11.600
Outer race inner radius	RORI	17.900
Outer race raceway radius	RORW	17.925
Outer race outer radius	RORO	20.300
Properties (AISI 51200 steel)		**Value**
Thermal conductivity (W/m-K) (20-200°C)		46.6
Coefficient of thermal expansion (μm/m-°C) (23-280°C)		11.9

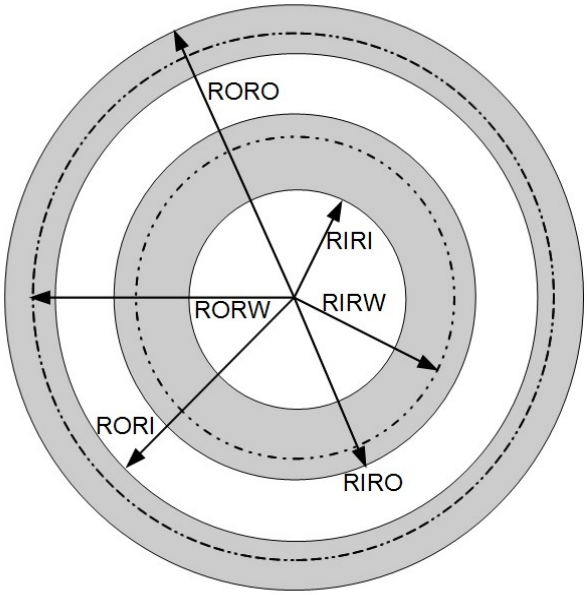

Figure 6: Bearing dimensions.

The motor used to spin the shaft is a 12 V motor similar to those used in cordless drills. The motor can deliver up to 150 in-lb of torque, though for this project it is doubtful that this was ever required due to the very low load on the motor. The motor never drew over 3.5 A during operation, in part due to the low angular velocities were required for this project.

As the ungeared motor ran at higher angular velocities than desired it was geared down to produce angular velocities in the proper range. The motor gear has 16 teeth and the shaft gear has 42 teeth, leading to a 0.318:1 gear ratio. For this experiment, therefore, the motor runs at between 850 and 2000 rpm. During operation the motor had a deadband where the shaft only began to spin after a certain current was applied. This current changed; in fact, despite the fact that the experiment configuration did not change from day to day, no good correlation was achieved between current and angular velocity. The cause for this is unknown.

The shaft was double-wrapped in Armacell Tubolit polyethylene foam insulation, giving a total insulation thickness of 1.5 cm. A cap of insulation of the same thickness was placed over

the top of the shaft. The thermal conductivity of the foam is 0.04 W/m-K [25]. After heating the shaft to test temperature and letting it reach steady state, the outer diameter of the insulation was at room temperature, which was one of the checks used to ensure that enough insulation was used. Electrical tape was used to hold the insulation in place.

The heater could not be connected to a stationary power source due to the rotation of the shaft. The heater was therefore powered by a 9V battery attached to the side of the shaft. The battery was replaced periodically over the course of the tests. As stated above, the battery voltage was measured and recorded at the beginning and end of each test. The voltage used to calculate the heater power was found from the average of the average of the beginning and end voltage and the end voltage as seen in the following equation.

$$V = \frac{\frac{V_{beg} + V_{end}}{2} + V_{end}}{2} \tag{18}$$

Here V is voltage and the subscripts *beg* and *end* denote voltages measured at the beginning and end of the test, respectively. Taking the voltage averages in this manner was done because the bearing was in a steady-state condition during the last half of the test, and battery characterization tests showed that there is a very steep voltage change at the beginning of the test time. However, the change in voltage flattened out toward the latter end of the test. Figure 7 shows an example of a battery characterization test. The time period between 300 and 600 seconds represents the time during a bearing test when the system has reached steady state.

The heater used is a Kapton® Polymide film flexible heater from Omega. It is 2.5 cm by 5 cm and outputs 20 W at 28 V. Since the largest battery it was practical to attach onto the shaft was a 9V battery, the total output power was not high. The actual output power was calculated for each test using the electrical resistance of the heater R, which was measured as 38.8 Ω at 45°C,

the measured average voltage of the battery V, and the formula for power (q) from [28].

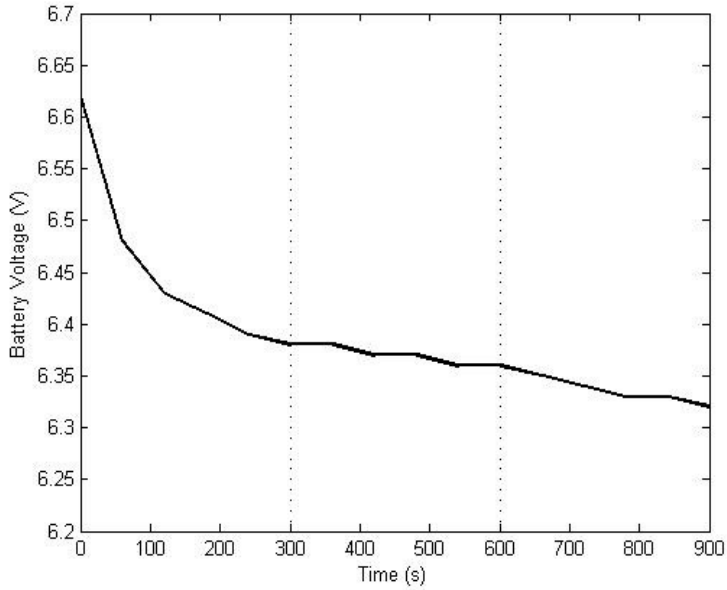

Figure 7: Battery characterization test.

$$q = \frac{V^2}{R} \tag{19}$$

Using a higher voltage heater for a bigger heat flow was considered impractical within the budget available for this experiment. If a large heat flow is required, one would probably have to use a slip ring assembly to ensure enough power is being delivered to the heater.

One consideration for this project is that not all of the heat flows out through the bearing, as there is no insulating material between the shaft and the shaft gear. Future studies may wish to cap this gear with a PVC cap in addition to/in place of the copper end cap used to connect the shaft gear to the shaft. For this study experiments to determine the steady-state temperature of the shaft were conducted, and this was used to calculate an average thermal resistance for the shaft. The shaft thermal resistance and the bearing thermal resistance were then used to calculate the heat flow through each component.

Experimental Procedure

To ensure repeatability a set procedure was used for every test. The procedure is as follows.

1. Examine experimental apparatus to ensure connections are tight, batteries are good, etc.
2. Open TC Central (thermocouple data acquisition system).
3. Turn on shaft and outer race wireless thermocouple transmitters. Make sure they are transmitting and that the battery power is good (front page of TC Central).
4. Hook up power supply to the heater leads. Turn power supply on and adjust voltage to ~18 V.
5. Watch the data acquisition system. When the shaft temperature reaches 40ºC begin recording data by pressing "Start" on the Data Log page. Make sure to change the data file name so previous test files are not overwritten.
6. When the shaft temperature reaches 55ºC reduce power supply voltage to 0 V.
7. Connect the heater and the 9 V battery.
8. Measure and record battery voltage.
9. Connect the power supply to the motor.
10. Dial in the test run current. Make sure the motor is on the constant current mode of operation (green "CC" visible on display).
11. Record the current.
12. Set a 10 minute timer. Record the time the timer starts. This is to assist in finding the steady state time later.
13. Using the camera and tripod, take a 30-40 s video of the motor so the rotational speed can be determined later. Mention on the video the date, run number, and

current.

14. As the experiment runs, watch the voltage/current and temperature on the data acquisition system. Note that on the thermocouple DAQ straight lines for both the shaft and outer race temperature indicate steady state. Also note they may decrease at the same rate with the outer race lagging slightly behind the shaft. This is another indicator of steady state.
15. When the timer finishes record the time. This is to assist in finding the steady state time.
16. Set the current to 0 A so the motor stops.
17. Measure and record the 9 V battery voltage.
18. Disconnect the shaft heater.
19. Let the bearing cool down.
20. Turn off DAQ.
21. If another run is scheduled, repeat steps 4-20.
22. Turn off thermocouple transmitters.
23. Turn off power supply.
24. Exit TC Central
25. Secure test setup.

Data Reduction and Analysis

The bearing thermal resistance was calculated by measuring the temperature difference across the bearing and dividing by the input power. This method of calculating the thermal resistance is similar to the approach taken by Haas and Nissan in [29]. Recall that the bearing input power is not the same as the heater power due to conduction out through the shaft gear.

The resistance was plotted against revolutions per minute to see if there was a correlation.

This correlation will be discussed further in the Results section. The angular velocity was plotted against the current to see if a correlation occurred. Generally speaking, the angular velocity increased with increasing current, but no correlation that would enable motor speed to be definitively plotted against current was found.

Heat flow through the shaft and out of the shaft bearing was determined to be a significant heat flow path in the system. Accordingly, several test runs were conducted to determine the thermal resistance of the shaft. Knowing the thermal resistance of the shaft enables an estimate to be made of the percentage of the total heat that flows through the bearing. The method used to determine the thermal resistance of the shaft was identical to that used to calculate the thermal resistance of the bearing. Temperature data were taken with the shaft spinning at various angular velocities. The battery voltage was also recorded and the heater power calculated. The shaft thermal resistance was then calculated by dividing the temperature difference by the input power and plotted against the shaft angular velocity.

RESULTS AND DISCUSSION

The following section compares the results from the experiment with the calculations from the MATLAB code. The results are followed by an uncertainty analysis for both the experiment and the code.

Analytic vs. Experimental Comparisons

As mentioned in the Experimental Validation – Experimental Apparatus section, not all of the heat flows out through the bearing. To find the percentage of the heat flow through the bearing, the bearing and shaft thermal resistances were first calculated using the full heat flow value (Figure 8).

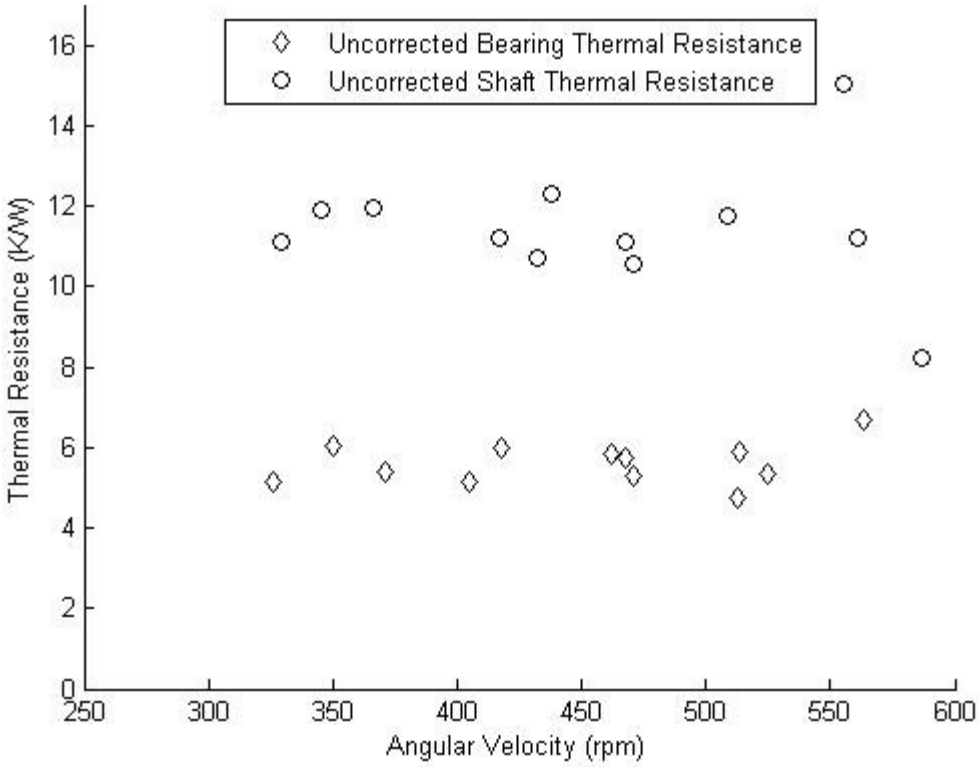

Figure 8: Uncorrected bearing and shaft thermal resistances.

From Figure 8 one can see that the bearing thermal resistance is about half of the shaft thermal resistance. Using the heat transfer equivalent of the current divider rule we find that, using the average value of 11.4 K/W for the shaft thermal resistance, the heater power splits with about 66% transferring out through the bearing and the other 34% through the shaft. The average shaft thermal resistance value was used to calculate all heater power splits because, due to the difficulty in selecting an exact angular velocity, the shaft velocities for the bearing and shaft tests did not line up exactly. The uncertainty due to using the average shaft thermal resistance is approximately 7.9%.

The heater power of each bearing test is multiplied by the thermal resistance percentage, and the bearing thermal resistance recalculated using the corrected heat flow value. Figure 9 shows bearing thermal resistance from the experiment plotted against calculated bearing thermal resistance. The calculated thermal resistance used the full correlation; that is, both Couette/Taylor-Couette flow and Dean flow thermal resistances were considered.

The data scatter in Figure 9 makes it impossible to calculate a trend of the bearing resistance as a function of angular velocity. However, mean magnitude of the thermal resistance data does show that reducing the power by approximately 34% due to shaft heat conduction adjusts the experimental data to agree significantly better with the Full Correlation resistance model. A factor that may be contributing to the large measured thermal resistance data scatter is premature transition from laminar to turbulent flow even with the low flow Reynolds numbers. There are many flow perturbation sources that might cause the flow to transition. The fact that the bulk of the thermal resistance values are lower than the correlation seems to indicate that the flow has transitioned. Thermal resistance for a turbulent flow is expected to be lower than that for a laminar flow. The analytical algorithm is built from laminar correlations, and so thermal resistance values that are lower than the correlation could indicate that the flow is turbulent.

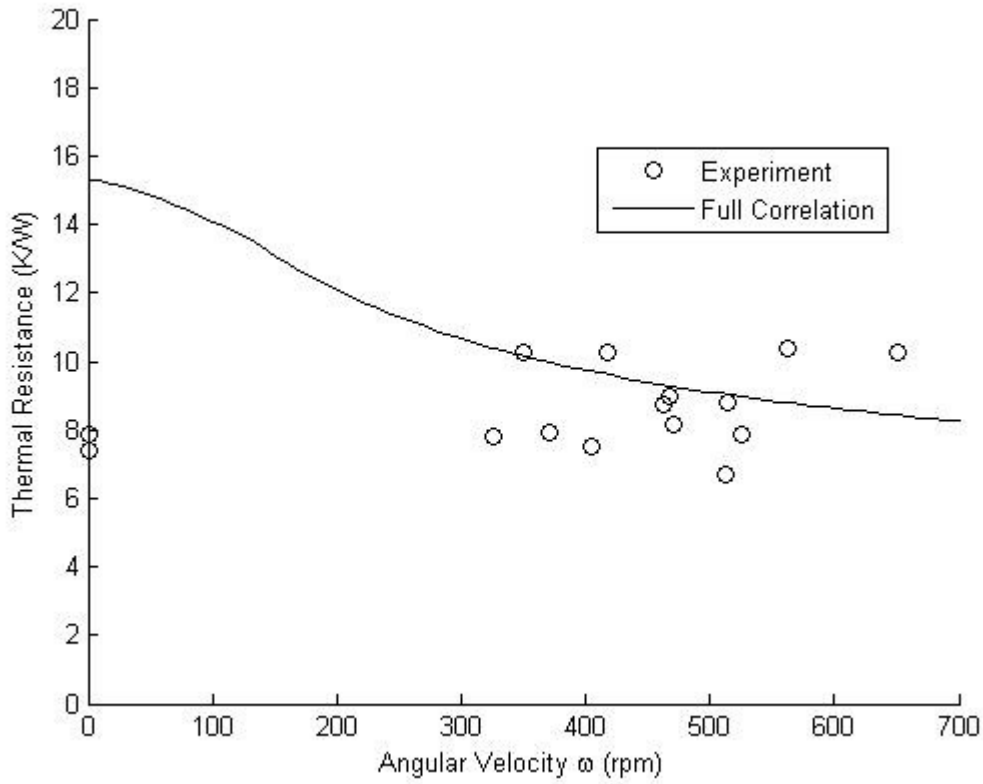

Figure 9: Bearing thermal resistance vs. angular velocity.

A possible justification for the turbulent flow argument is found from Farouk et al. [30]. Farouk discusses the convective flows around a rotating isothermal cylinder. In it, the authors point out that for small values of $\sigma = Gr/Re^2$ the flow around an isothermal cylinder rotating in an infinite fluid tends to transition to turbulence. This study has a small Grashof number due to the small gap diameter, which makes the Reynolds number at which the flow would begin to transition in this case less than $Re = 10$. This flow scenario is not exactly analogous to that found in [30]; however, it is something to consider. The influence of the outer race will have an impact on the flow, and since this transition is not considered in the Taylor flow scenarios studied in the literature survey, the influence of σ may not have as much of an effect on the bounded flow as it does for the unbounded flow.

Figure 10 shows the analytical convection coefficients. As expected the convection coefficient is constant in the Couette flow regime below the critical Taylor number. The Dean flow convection coefficient increases from the outset. It is interesting to see how much larger the Dean convection coefficient is than the Taylor-Couette coefficient. The larger Nusselt number is due to the presence of the Dean secondary flow caused by the curvature of the raceway.

Uncertainty Analysis

Results without knowledge of their uncertainty are useless. Therefore, the uncertainty for both the analytic and experimental thermal resistance were calculated. The process and results are discussed below.

The analytic thermal resistance will be discussed first. Uncertainties on properties used in this analysis are given in Table 6. These properties were taken from available reference sources, not calculated. References are given in brackets next to the property.

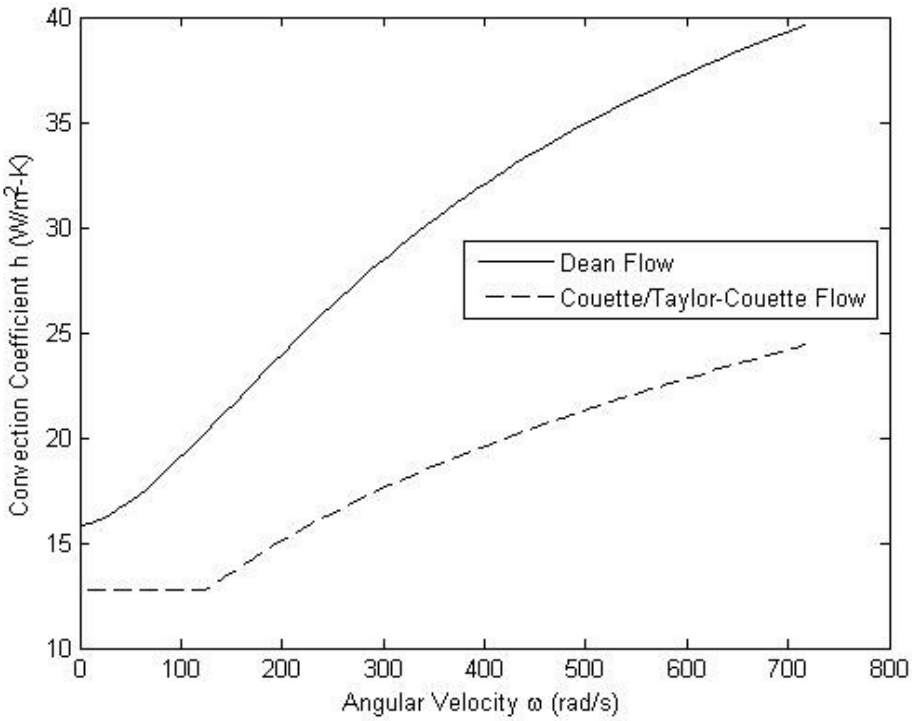

Figure 10: Convection coefficients vs. angular velocity.

Table 6: Analytic Correlation Properties and Uncertainties

Property	**Ref.**	**Systematic Uncertainty**	**Random Uncertainty**
Inner Race Dimensions	[31]	$9 \cdot 10^{-6}$ m	0
Outer Race Dimensions	[31]	$12 \cdot 10^{-6}$ m	0
Steel Thermal Conductivity	[22]	5%	0
Air Thermal Conductivity	[32]	1%	0
Air Viscosity	[33]	0.4%	0
Prandtl Number	[19]	5%	0
Air Volumetric Thermal Expansion Coefficient	[19]	1 1/K	0
Temperature Measurements	[34]	0.5°C	0.5°C

The bearing ball diameter uncertainty and the bearing length uncertainty are the same as the inner race uncertainty. These values were taken from [31], as were the dimensions for the ball bearing. Note that in some cases, specifically for the Prandtl number and the bearing steel thermal conductivity, no uncertainty estimates were found. Prandtl numbers can vary widely for lamnar, turbulent, and transitional flow, and no formal uncertainty model exists, and the bearing steel thermal conductivity does not seem to have been studied in depth. These uncertainties were therefore assumed to be 5% of the property value.

Uncertainties on other quantities were calculated. In general, the uncertainties for the dimensionless numbers are not considered to vary with angular velocity, as we are picking the angular velocity in the code and assuming the uncertainty in the angular velocity is zero. Representative values for the Nusselt number uncertainties, which do vary with angular velocity, are listed in Table 7. These values are on the high end of the uncertainties. All uncertainties are listed in percent form (i.e. u_{Gr}/Gr). These values are very small, which is not surprising for the values that depend on bearing geometry – the tolerances are very small – but the small uncertainties were unexpected for the other values. The low uncertainty values can be explained in part by the fact that the expressions for the Nusselt number correlations and their derivatives

Table 7: Calculated Properties' Uncertainties.

Property	Vary?	Uncertainty
Grashof Number	No	0.0023%
Reynolds Number	No	0.37%
Dean Number	No	0.38%
Taylor Number	No	0.62%
Couette Nusselt Number	No	0.034%
Taylor-Couette Nusselt Number	Yes	0.54%
Dean Nusselt Number	Yes	0.013%
Taylor-Couette Convection Area	No	0.24%
Dean Convection Area	No	0.18%

are very complicated. Since uncertainties can be calculated from the general formula [35]

$$u_y = \left[\left(\frac{\partial y}{\partial x_1} \right)^2 u_{x_1}^2 + \left(\frac{\partial y}{\partial x_2} \right)^2 u_{x_2}^2 + \ldots + \left(\frac{\partial y}{\partial x_n} \right)^2 u_{x_n}^2 \right]^{1/2} \tag{18}$$

it can be seen that if the partial derivatives are very complex uncertainties may feed into each other or cancel each other out. It is suspected that this is the case for the Nusselt number correlations.

The final thermal resistance uncertainty values for the code are listed in Table 8. As these resistances depend on properties calculated in the code (Taylor number, Dean number, etc.) they are representative values listed as percentages. The “Overall” quantity is the 95% confidence level value of the uncertainty.

It can be seen for the inner and outer races the largest contributor to the uncertainty is the thermal resistance of the steel. No data were found that describe the uncertainty on the thermal conductivity. Another major contributor to the uncertainty is the Prandtl number.

Table 8: Uncertainty of Resistances

Resistance	Uncertainty
Inner Race	5.01%
Outer Race	5.05%
Bearing Ball	5.00%
Taylor Section	7.22%
Dean Section	5.28%
Overall	8.78%

Table 9 shows the experimental parameters and their associated uncertainties. Data were collected for ten minutes for each angular velocity. The long experiment run time allowed the bearing to come to steady state and then have about 300 seconds of steady-state run time, which in turn allowed the temperature to be calculated with a fairly low standard deviation. This standard deviation was used with the number of samples to calculate the systematic uncertainty for the temperature.

For the battery voltage, an approximation was used that averaged the average voltage over the whole run with the end voltage as described in the Experimental Validation – Experimental Apparatus section. The voltage was calculated this way to provide a better estimate of the voltage during the bearing's steady-state phase. Though this generates some uncertainty in the voltage, when looking at various charts and the battery characterizations it can be seen that the voltage varies about 0.02 V end-to-end or ±0.01 V. These uncertainties were root sum squared together to obtain the value shown in the chart.

The random uncertainty for the camera comes from the camera frame rate of 30 frames/s. This corresponds to 0.033 s/frame, so when calculating the angular velocity from the video footage the uncertainty in the time is half that.

Table 9: Experiment Uncertainties

Property	**Ref.**	**Systematic Uncertainty**	**Random Uncertainty**
Angular Velocity	--	0	0.5 rev/s
Frame Rate of Camera	[36]	0	0.017 s
Voltage	[37]	0.05% + 0.01V	0.051 V
Resistance	[37]	0.8% + 0.04 Ω	0.05 Ω
Temperature	[34]	$\frac{\sigma_x}{\sqrt{(N)}}$	0.5°C

Combining the uncertainties, the total uncertainty for the experiment ranges from 2.42% to 5.29% in the 95% confidence level. This is quite low for an experiment, and does not account for the differences between the model and experiment. Clearly there are a number of unmodeled heat flow paths in the experiment that are not properly accounted for. These may include heat flow through the copper shaft into the motor gear and axial heat flow through the bearing into the bearing retainer plates. Though the shaft was heavily insulated, a small amount of heat may also have transferred through the insulation.

We know that heat flows through the copper shaft into the motor gear. The uncertainty on these experimental resistances will be the same as that on the bearing thermal resistances as the thermal resistances are found in the same way. This raises the overall uncertainty to about 8%. Though there are doubtless more unmodeled heat flow paths, the further analysis of heat transfer through the shaft contributes a better knowledge of the overall system characteristics.

Figure 11 is a plot of the uncertainty on the correlation and the data. The values are in the 95% confidence level. Note that as the angular velocity is larger the analytic uncertainty also increases; this is due to the complicated derivatives for the Dean and Taylor-Couette Nusselt number correlations causing parameters like the Dean number to appear in the numerator of the total uncertainty.

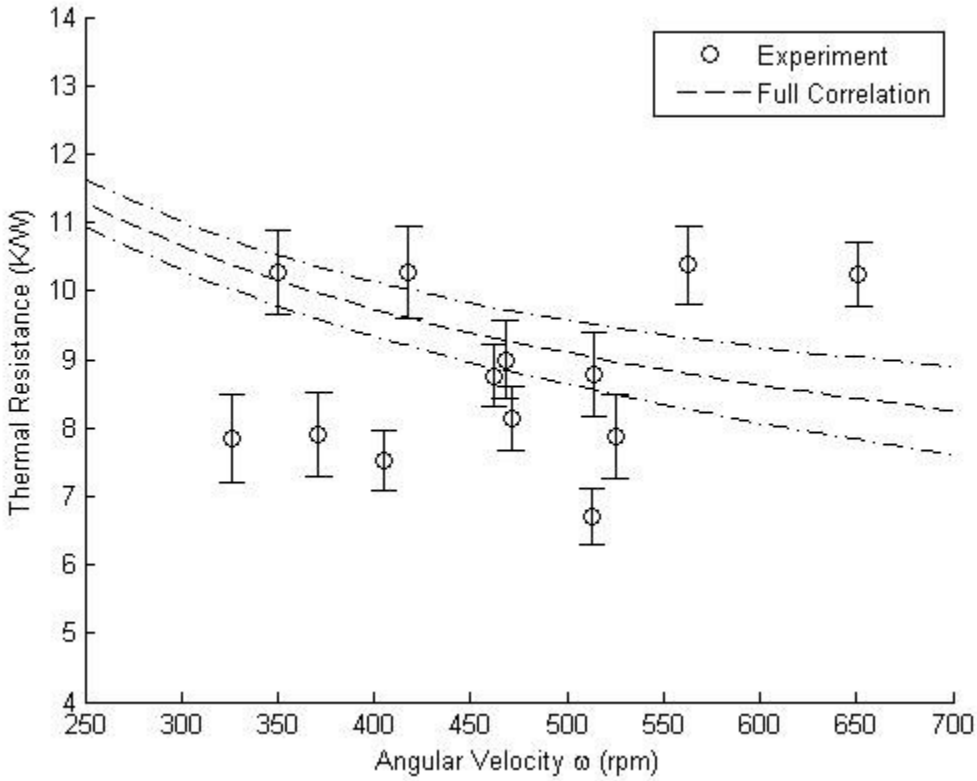

Figure 11: Uncertainty on the data.

As stated before, it was expected that the experimental thermal resistances would be lower than the calculated thermal resistances due to the computer algorithm being based on laminar flow correlations. It is also interesting to note that there is not a definite pattern to the error bars in Fig. 11. This seeming incongruity can be traced in part to the 9 V battery used for the heater power. The battery was run until its starting voltage was below 7 V. Due to the way the uncertainty equations played out, the test runs with a lower starting voltage will, in general, have a lower overall thermal resistance uncertainty. Note that the uncertainty depends on both the shaft and bearing thermal resistance tests.

CONCLUSIONS

For this project a MATLAB program was written to calculate the thermal resistance of a single row angular contact ball bearing using the resistances of the bearing structure and the convection coefficients of the fluid inside the bearing. An experiment to test the program was executed and the results were found to correlate within some uncertainty bounds. The result of this project is a basic code that provides a first-order approximation of the heat transfer capabilities of a bearing at low Reynolds numbers.

A thermal resistance model of a ball bearing rotating on a heated inner shaft is built using the resistances from the bearing races, bearing balls, and convection occurring inside the bearing. It was determined from a literature survey that circular Couette/Taylor-Couette flow can be used for the flow between the bearing races and Dean flow can be used for the flow in the raceway. A code to determine the thermal resistance of a bearing depending only on its geometry and the angular velocity of the shaft was written in MATLAB.

The code was tested using an experimental apparatus designed to calculate the thermal resistance of the bearing by measuring the temperature drop between the shaft and the outer race. The heated shaft was rotated at several angular velocities corresponding to the Reynolds number range of interest. Once the tests were complete the experimental data were plotted against the calculated data. The experimental bearing thermal resistance magnitudes are seen to be similar to those calculated with the MATLAB program.

Future experiments of this type may wish to use a slip ring arrangement instead of the wireless thermocouple and 9V battery powered heater used in this experiment. While the arrangement worked well for this experiment, if a larger temperature drop is desired a bigger heater will be needed; this will necessitate a larger voltage. Since it is not practical to attach a much larger battery to the shaft, an alternate means of supplying the voltage is needed, and a slip ring will be the most simple method.

Another way to expand on this work is by testing several different bearings instead of just one. This is the best way to rigorously test the code and ensure that the semi-agreement between the code and the experiment is not just a surprising coincidence.

Bearings operating at low angular velocities can act as a primary heat flow path for even simple systems. The thermal resistance of these bearings can be calculated experimentally or an estimate can be made using the MATLAB program developed for this project. This program is based on laminar flow correlations which may result in a conservative value for the thermal resistance. Further work should include testing more bearings at a higher heat flow.

REFERENCES

1. Couette, M., "Etudes sur le frottement des liquides," *Annales de Chimie et de Physique serie VI*; Vol. 21, 1890, pp. 433-510.
2. Hwang, Jo., and Yang, K., "Numerical Study of Taylor-Couette flow with an axial flow," *Computers & Fluids*; Vol. 33, 2004, pp. 97-118.
3. Harris, T.A., *Rolling Bearing Analysis*, John Wiley & Sons, New York, 1966.
4. Kim, A., and Lee, S., "Prediction of thermo-elastic behavior in a spindle-bearing system considering bearing surroundings," *International Journal of Machine Tools & Manufacturer*, Vol. 41, 2001, pp. 809-831.
5. Busam, S., Glahn A., and Wittig, S., "Internal Bearing Chamber Wall Heat Transfer as a Function of Operating Conditions and Chamber Geometry," *Transactions of the ASME*, Vol. 122, 2000, pp. 314-320.
6. Constantinescu, V.N., Laminar Viscous Flow, Springer-Verlag, New York, 1995.
7. Ahmed, N., *Fluid Mechanics*, Engineering Press, Inc., San Jose, CA, 1987.
8. Munson, B.R., Young, D.F., and Okiishi, T.H., *Fundamentals of Fluid Dynamics*, 3rd ed., John Wiley & Sons, Inc., New York, 1998.
9. Kundu, P.K. and Cohen, I.M., *Fluid Mechanics*, 4th ed., Academic Press, Burlington, MA, 2008.
10. Kreith, F., "Convection Heat Transfer in Rotating Systems," *Advances in Heat Transfer*, Vol. 5, 1968, pp. 129-251.
11. Ball, K.S., Farouk B., and Dixit, V. C., "An experimental study of heat transfer in a vertical annulus with a rotating inner cylinder.," *International Journal of Heat and Mass Transfer*, Vol. 32, 1989, pp. 1517-1527.
12. Panton, R.L., *Incompressible Fluid Flow*, John Wiley & Sons, Inc., New York, 1984.
13. Chen, Y., Chen, H., Zhang, J., and Zang, B., "Viscoelastic flow in rotating curved pipes,"

Physics of Fluids, Vol. 18, 2006, pp. 1-17.

14. Rosenow, W. M., Harnett, J.P., and Cho, Y.I., *Handbook of Heat Transfer,* 3rd ed., McGraw-Hill, New York, 1998.
15. Fellouah, H., Castelain, C., El Moctar A.O., and Peerhossaini, H., "A criterion for detection of the onset of Dean instability in Newtonian fluids," *European Journal of Mechanics B/Fluids*, Vol. 25, 2006, pp. 505-531.
16. Naphon, P., and Wongwises, S., "A review of flow and heat transfer characteristics in curved tubes," *Renewable and Sustainable Energy Reviews*, Vol. 10, 2006, pp. 463-490.
17. Wang, L. and Cheng, K.C., "Flow in curved channels with a low negative rotation speed," *Physical Review E*, Vol. 51, 1995, pp. 1155-1163.
18. Kreith, F., Roberts L.G., Sullivan J.A., and Sinha S.N., "Convection Heat Transfer and Flow Phenomena of Rotating Spheres," *International Journal of Heat and Mass Transfer*, Vol. 6, 1963, pp. 881-895.
19. Incropera, F.P., Dewitt, D.P., Bergman, T.L., Lavine, A.S., *Fundamentals of Heat and Mass Transfer*, 6th ed., John Wiley & Sons, Inc., Hoboken, NJ, 2007.
20. "AISI E 52100 Steel." *MatWeb Material Property Data.* MatWeb, LLC. Web. 7 Nov. 2011.
21. Mizuta, K., et al. "Heat Transfer Characteristics Between Inner and Outer Rings of an Angular Ball Bearing," *Transactions of the JSME: Series B*, Vol. 66, 2000, pp. 1162-1169.
22. Yovanovich, M.M., "Thermal Constriction Resistance Between Contacting Metallic Paraboloids: Application to Instrument Bearings," *Heat Transfer and Spacecraft Thermal Control*, edited by J.W. Lucas, Vol. 24, Progress in Aeronautics and Astronautics, AIAA, Reston, VA, 1971, pp. 337-358.
23. Bairi, A., Alilat N., Bauzin J.G., and Laraqi, N., "Three-dimensional stationary thermal

behavior of a bearing ball," *International Journal of Thermal Sciences*, Vol. 43, 2004, pp. 561-568.

24. Aoki, H., Nohira, H., and Arai, H., "Convective Heat Transfer in an Annulus with an Inner Rotating Cylinder," *Bulletin of JSME*, Vol. 10, 1967, pp. 523-532.
25. "The Copper Tube Handbook." *Copper.Org.* Copper Development Association, 2011, http://www.copper.org/publications/pub_list/pdf/copper_tube_handbook.pdf, [cited 11 November 11].
26. "Annealed Copper." *MatWeb Material Property Data.* MatWeb, LLC., http://www.matweb.com/search/datasheet.aspxmatguid=9aebe83845c04c1db5126fada6f76f7e&ckck=, [cited 1 November 2011].
27. "Tubolit." *Armacell Advanced Insulation.* Armacell Enterprise GmbH, 2011, http://www.armacell.us/www/armacell/ACwwwAttach.nsf/ansFiles/051-001-NA(NA).pdf/$File/051-001-NA(NA).pdf, [cited 11 November 11].
28. Boylestad, R.L., *Introductory Circuit Analysis*, 11th ed., Pearson Prentice Hall, Upper Saddle River, NJ, 2007.
29. Haas, F.C., and Nissan A.H., "Experimental Heat Transfer Characteristics of a Liquid in Couette Motion and with Taylor Vortices," *Proceedings of the Royal Society of London. Series A, Mathematical and Physical Sciences*, Vol. 261, 1961, pp. 215-226.
30. Farouk, B., and Ball, K.S., "Convective flows around a rotating isothermal cylinder," *International Journal of Heat and Mass Transfer*, Vol. 28, 1985, pp. 1921-1935.
31. "Rolling Bearings." *NSK.com*. NSK Motion and Control, 2005, http://www.nskamericas.com/cps/rde/xbcr/na_en/e1102i.pdf, [cited 18 November 2011].
32. Kadoya, K., Matsunaga N,, and Nagashima, A., "Viscosity and Thermal Conductivity of Dry Air in the Gaseous Phase," *Journal of Physical Chemistry Reference Data*, Vol. 14, 1985, pp. 947-970.

33. Kestin, J. and Whitelaw J.H., "The viscosity of dry and humid air," *International Journal of Heat and Mass Transfer*, Vol. 7, 1964, pp. 1245-55.

34. "User's Guide: MWTC/MWRTD Series Wireless Thermocouple/RTD Connector/Transmitter & Receivers." Omega Engineering, Inc., 2010.

35. Coleman, H.W., and Steele, W.G., *Experimentation, Validation, and Uncertainty,* 3rd ed., John Wiley & Sons, Inc., Hoboken, NJ, 2009.

36. "Advanced Camera User Guide: Canon PowerShot SD600 Digital Elph." Canon, 2006.

37. "Ideal Industries Inc. Technical Manual Model 61-310." Ideal Industries Inc., 2007.

38. Dikmen, E., van der Hoogt, P., de Boer, A., Aarts, R., and Jonker, B., "Thermal Modeling of a Mini Rotor-Stator System," *Proceedings of the ASME 2009 International Mechanical Engineering Congress & Exposition*, ASME, Lake Buena Vista, FL, 2009, pp. 13-19.

APPENDICES

MATLAB Driver Code

```
% Bearing_Thermal_Resistance

% This program calculates the thermal resistance for a ball bearing
that is
% spinning on a heated shaft using a combination Dean/Couette flow
% correlation along with the thermal resistance from the bearing races
and
% balls.

clear all; close all; clc

% Note that these temperatures are estimates so we can calculate fluid
% properties.
T_s = 50+273.15;        % Shaft temperature, K
T_r = 40+273.15;        % Outer race temperature, K
Tave = (T_s+T_r)/2;     % Average temperature in the raceway/ring gap, K
nu = 1.7462e-5;         % Kinematic viscosity m^2/s
ksteel = 54;            % Thermal conductivity of steel, W/m-K AISI
52100
                        % Found from Basu, Chakraborty, Shariff, etc.

% Calculate the thermal conductivity of air at the mean temeperature
% Logan pressure at altitude is 86008 Pa
% Data from Kadoya et al
k300 = 26.20+(26.23-26.20)/(0.1-0.01)*(.086-0.01);
k350 = 29.81+(29.84-29.81)/(0.5-0.1)*(.086-0.01);
kair = (k300 + (k350-k300)/(350-300)*(Tave-300))/1000;

ctes = 11.9e-6;         % Coefficient of thermal expansion, um/m/deg-c
                        % Data from Matweb
heatr = 38.8;           % Heater electrical resistance, Ohm @45 deg C
                        % Measured in lab

g = 9.81;               % Acceleration due to gravity, m/s
Ta_crit = 1708;         % Critical Taylor number (fluid transitions
from
                        % Couette flow to Couette flow with vortices)
Pr = 0.7047;            % Prandtl number for air, found from Incropera
beta = 1/Tave;          % Coefficient of volumetric thermal expansion,
1/K

% Input bearing dimensions
roro = 0.0201;              % Outer race outer radius, m
rori = 0.0179;              % Outer race inner radius, m
riro = 0.0116;              % Inner race outer radius, m
riri = 0.006;               % Inner race inner radius, m
db = 0.25*0.0254;           % Raceway/ball diameter, m
lb = 0.0135;                % Bearing length, m
drace = rori-riro;          % Ring/race gap width, m
cr = db*0.55;               % Raceway curvature, m (this is the RADIUS
                            % of the raceway, note). Rule of thumb.
```

```
nball = 8;                  % Number of bearing balls (counted)

% Matrix so the velocity profile in the ring gap can be calculated
arr = riro:(rori-riro)/100:rori;

% Calculate other bearing dimensions
rb = db/2;                      % Raceway/ball radius, m
rbth = acos(((db-drace)/2)/rb); % Angle of race/ball contact to find
                                % bearing section lengths
L2 = 2*rb*sin(rbth);            % Length of Dean section
L1 = (lb-L2)/2;                 % Length of Taylor-Couette section
rmean = (riro+rori)/2;          % Mean radius of the bearing race, m
rirw = riro-(db-drace)/2;       % Raceway inner radius, m
rorw = rori + (db-drace)/2;     % Raceway outer radius, m

% Recognize that you're going to have to split the bearing into three
% sections. Two will be exactly the same, and the other will be the
raceway
A1 = 2*pi*L1*(riro+rori);       % Couette flow area, m^2
A2 = pi*db*2*pi*rmean;          % Surface area of the Dean flow area,
m^2

%-----------------------------------------------------------------------
----
% Contact patch calculations
% This section will calculate the contact patch area for the bearing
balls.
% It requires dimensions in English units. Equations drawn from Machine
% Design 3rd Ed by Robert L. Norton

% Dimensions
R1 = db/(2*0.0254);         % radius of curvature - bearing ball, in
R1p = db/(2*0.0254);        % radius of curvature - bearing ball in
                            % perpendicular frame, in
R2 = cr/0.0254;             % radius of curvature - raceway, in
R2p = rorw/0.0254;          % radius of curvature - inner race, in

% Geometry constants - this is assuming that the patch area for the
inner
% and outer races are the same. Not true, but we will approximate for
ease
% of finding the thermal resistance.
A = 1/2*(1/R1 + 1/R1p + 1/R2 + 1/R2p);
B = 1/2*((1/R1-1/R1p)^2+(1/R2-1/R2p)^2+2*(1/R1-1/R1p)*(1/R2-1/R2p)*...
    cos(2*0))^(1/2);
phi = acos(B/A)*180/pi;

% Material constants
E = 29700000;           % Modulus of elesticity, psi
poi = 0.290;            % Poisson's ratio
m12 = (1-poi^2)/E;      % Material constants. Balls and bearing are
made of
                        % same materials, so the material constants are
                        % the same.
```

```
F = 150;                  % Axial load, lb
ka = 1.202+(1.128-1.202)/(80-75)*(phi-75);      % From textbook pg 445
kb = 0.846+(0.893-0.846)/(80-75)*(phi-75);      % From textbook pg 445

% Calculate the areas
aa = ka*(3*F*2*m12/(4*A))^(1/3);    % Major axis, in
bb = kb*(3*F*2*m12/(4*A))^(1/3);    % Minor axis, in
apatch = pi*aa*bb;                  % Area of the patch, in^2
aam = aa*0.0254;                    % Major axis, m
bbm = bb*0.0254;                    % Minor axis, m
apm = pi*aam*bbm;                   % Patch area, m^2

Rth_bal = db/(ksteel*apm);          % Thermal resistance of one bearing
                                    % ball, W/m-K

%-----------------------------------------------------------------------
----
% Uncertainty Analysis
% This next section will help us prepare for the uncertainty analysis.
% Uncertainties that we know
u_or = 12*10^-6;                    % Outer race tolerance
u_ir = 9*10^-6;                     % Inner race and length tolerance
ukks = 0.05;                        % Estimated Uncertainty on steel,
uk/ks
ut = 0.5;                           % Thermocouple random uncertainty
ununu = 0.002;                      % Uncertainty on nu, u_nu/nu
uprpr = 0.05;                       % GUESS uncertainty on Pr, u_Pr/pr
uww = 0;                            % We're setting the angular
velocity,
                                    % so we assume the uncertainty is 0.
ukka = 0.01;                        % Uncertainty on thermal
conductivity
                                    % of air, uk/ka

% Calculate some constant thermal resistances
% Thermal resistance uncertainty U_Rth/Rth of the inner race: Section 1
urthrth_ir_1 = sqrt((1/(riro*log(riro/riri)))^2*u_ir^2 + ...
    (1/(riri*log(riro/riri)))^2*u_ir^2 + (u_ir/L1)^2 + (ukks)^2);

% Thermal resistance uncertainty U_Rth/Rth of the inner race: Section 2
urthrth_ir_2 = sqrt((1/(rirw*log(rirw/riri)))^2*u_ir^2 + ...
    (1/(riri*log(rirw/riri)))^2*u_ir^2 + (u_ir/L2)^2 + (ukks)^2);

% Thermal Resistance Uncertainty U_Rth/Rth of the outer race: Section 1
urthrth_or_1 = sqrt((1/(roro*log(roro/rori)))^2*u_or^2 + ...
    (1/(rori*log(roro/rori)))^2*u_or^2 + (u_ir/L2)^2 + ukks^2);

% Thermal Resistance Uncertainty U_Rth_Rth of the outer race: Section 2
% Note that u_ir is used in the first term because the dimension of rorw
% depends on the bearing ball, which has the uncertainty u_ir
urthrth_or_2 = sqrt((1/(rorw*log(roro/rorw)))^2*u_ir^2 + ...
    (1/(roro*log(roro/rorw)))^2*u_or^2 + (u_ir/L2)^2 + ukks^2);

% U_rth/rth_bb of the bearing ball: per bearing ball
% Assume the bearing ball contact patch area uncertainty percent is the
```

```
% same as that of the iiner race.
urthrth_bb = sqrt(2*(u_ir/db)^2+ukks^2);

% Couette nusselt number uncertainty
% This still needs to be divided by the Nusselt number to get the total
% uncertainty U_Nu/Nu.However, it is constant because it depends only on
% geometry.
unu = sqrt(((2*riro*log(drace/riro+1)-2*drace/(drace/riro+1))/
(riro*log(drace/...
    riro+1))^2)^2*u_ir^2+((2*drace*riro^2/(drace+riro)*drace/
(drace+riro)^...
    2)/(riro*log(drace/riro+1))^2)^2*u_ir^2);

% Grashof number uncertainty u_Gr
ug = sqrt((ut*beta)^2+9*(u_ir/lb)^2+4*(ununu)^2);

% Reynolds number uncertainty u_Re/Re
urere = sqrt(uww^2+4*(u_ir/drace)^2+ununu^2);

% Taylor number uncertainty u_Ta/Ta
% Does not depend on w because we assume we know w exactly (it's a
% simulation)
utata = sqrt((u_ir/riro)^2+9*(u_ir/drace)^2+uww^2+4*ununu^2);

% Dean number uncertainty u_De/De
udede = sqrt(urere^2+1/4*(u_ir/drace)^2+1/4*(u_or/rmean)^2);

% Convection area uncertainties u_A/A
% Convection area uncertainty for Taylor-Couette flow
ua1a1 = sqrt((u_ir/(riro+rori))^2 + (u_or/(riro+rori))^2 + (u_ir/L1)^2);
% Convection area uncertainty for Dean flow
ua2a2 = sqrt((u_ir/db)^2 + (u_or/rmean)^2);
%-----------------------------------------------------------------------
----

% Move onto the main program where we will iterate over the angular
% velocity w.

n = 1;              % Counting variable

% Angular velocity loop
for w = 25:75   % This corresponds to RPMs between about 235 (25) and
720
                % (75)

% Velocity profile loop. This is for interest only and does not have any
% further use in the program.
for na = 1:size(arr,2);
vel_prof(na) = 1/(1-(riro/rori)^2)*((0-w*(riro/rori)^2)*arr(na)
+riro^2/...
    arr(na)*(w-0));
end

% Find the actual velocity in the center of the gap
% This is of interest because, though the correlations list the angular
```

```
% velocity of interest at the inner radius... but in this case the
velocity
% steadily decreases from the inner to the outer race.
nw = 1/(1-(riro/rori)^2)*((-w*(riro/rori)^2)*rmean+riro^2/rmean*w);

% Another way to calculate the mean velocity.
oth = mean(vel_prof);
% Reynolds number for the Taylor-Couette sections from Ref. 36.
Re_ta = w*riro*drace/nu;
% Reynolds number for the Dean section from Ref. 12
Re_de = db^2*w/nu;
% Taylor number for the Taylor-Couette section
Ta_ta = w^2*riro*drace^3/nu^2;

% Taylor number matrix, values calculated in RPM. This is for plotting
% purposes.
Tamat(n) = w*30/pi;

De = Re_de*sqrt(db/(2*rmean));     % Dean number (dimensionless)

% Calculate the thermal resistances for the solid parts of the bearing
% (meaning the races)
% Thermal resistance fo the inner race for the Taylor-Couette section
Rth_in_ta = log(riro/riri)/(2*pi*L1*ksteel);    % W/m-K
% Thermal resistance of the outer race for the Taylor-Couette section
Rth_out_ta = log(roro/rori)/(2*pi*L1*ksteel);   % W/m-K
% Thermal resistance of the inner race for the Dean section
Rth_in_de = log(rirw/riri)/(2*pi*L2*ksteel);    % W/m-K
% Thermal resistance of the outer race for the Dean section
Rth_out_de = log(roro/rorw)/(2*pi*L2*ksteel);   % W/m-K

Gr = g*beta*(T_s-T_r)*drace^3/nu^2;             % Grashof number

% Nusselt number for flows below the critical Taylor number
Nu_cond = 2*(drace/riri)/log(1+drace/riri);

% Select the Nusselt number based on the Taylor number for the
% Taylor-Couette flow section
if Ta_ta < Ta_crit
    Nu = Nu_cond;
else
    m = (Pr/Gr)^(1/6);
    Nu = Nu_cond*(Ta_ta/Ta_crit)^(m/2);
end

% Uncertainty in the Nusselt number for the Taylor-Couette section
unta = utafun(Ta_ta, Pr, Gr, unu, Nu_cond, utata, ug, uprpr);

% FYI Nusselt number of ball
% Nu_ball = 0.43*sqrt(Re_ball)*Pr^0.4
% Valid for Gr < 0.1*Re_ball, Re < 5e5, 0.7 < Pr < 217. This is for a
ball
% spinning in an infinite medium.

% Calculate thermal resistance of Taylor section
```

```
% Taylor convection coefficient W/m^2-K
h_ta = Nu*kair/drace;
% Convection coefficient uncertainty
uhtahta = sqrt((unta/Nu)^2 + (ukka)^2 + (u_ir/drace)^2);
% Taylor fluid thermal resistance, K/W
Rth_ta = 1/(h_ta*A1);
% Taylor-Couette thermal resistance uncertainty
urth_tarth_ta = sqrt(ua1a1^2 + uhtahta^2);

% Calculate the Nusselt number for the Dean flow section
% This is the Reynolds number where the Dean flow transitions to
turbulence
% in curved pipes.
Re_crit = 2100*(1+12*(rmean/drace)^(-0.5));

% First factor in calculating the Nusselt number
x1 = (1+957/(De^2*Pr));
% Second factor in calculating the Nusselt number
x2 = 1+0.477/Pr;
% Dean flow Nusselt number
Nu_de = ((3.657+4.343/x1)^3+1.158*(De/x2)^(3/2))^(1/3);
% Uncertainty on Dean flow values
[ux1 ux2 unude] = udeanfun(De, Pr, udede, uprpr, x1, x2);

% Calculate the thermal resistance of Dean section
h_de = Nu_de*kair/db;                % Dean convection coefficient,
W/m^2-K
% Dean convection coefficient uncertainty
uhdehde = sqrt((unude/Nu_de)^2 + (ukka)^2 + (u_ir/db)^2);
% Dean convection thermal resistance K/W
Rth_de = 1/(h_de*A2);
% Dean thermal resistance uncertainty
urth_derth_de = sqrt(ua2a2^2 + uhdehde^2);

% Bearing ball thermal resistance K/W
Rth_ball = Rth_bal/nball;

% Calculate the thermal resistances for each part of the bearing
% Thermal resistance of Taylor section
Rth_tcs = Rth_in_ta + Rth_ta + Rth_out_ta;
%Uncertainty of the Taylor section
ur_tcs = sqrt(urthrth_ir_1^2 + urth_tarth_ta^2 + urthrth_or_1^2);
% Thermal resistance of Dean section
Rth_ds = Rth_in_de + 1/(1/Rth_de+1/Rth_ball) + Rth_out_de;
% Uncertainty of the Dean section
ur_ds = sqrt((urthrth_ir_2*Rth_in_de)^2 + (((Rth_de+Rth_ball)*Rth_ball-
...
    Rth_de*Rth_ball)/(Rth_de+Rth_ball)^2)^2*(urth_derth_de*De)^2 +...
    (((Rth_de+Rth_ball)*Rth_de - Rth_de*Rth_ball)/
(Rth_de+Rth_ball)^2)...
    ^2*(urthrth_bb*Rth_ball)^2) + (urthrth_or_2*Rth_out_de)^2;

% Sum the thermal resistances in parallel to find the total thermal
% resistance for the bearing
Rth_total = 1/(1/Rth_tcs + 1/Rth_ds + 1/Rth_tcs);
```

```
u_total = sqrt((((2*Rth_ds+Rth_tcs)*Rth_tcs-Rth_tcs*Rth_ds)/(2*Rth_ds +
...
    Rth_tcs)^2)^2*ur_ds^2 + (((2*Rth_ds+Rth_tcs)*Rth_tcs-Rth_tcs*...
    Rth_ds)/(2*Rth_ds+Rth_tcs)^2)^2*(ur_tcs)^2);

% Now do matrixes so plotting can be done later
rthmat(n) = Rth_total;
rthmat2(n) = Rth_ds;
% Lines for 95% confidence around the thermal resistance lines
urthup(n) = Rth_total + 1.96*u_total;
urthdn(n) = Rth_total - 1.96*u_total;
urthup2(n) = Rth_ds + 1.96*ur_ds;
urthdn2(n) = Rth_ds - 1.96*ur_ds;
% Plots for convection coefficients
htamat(n) = h_ta;
hdmat(n) = h_de;
% Angular velocity matrix
wemat(n) = w*30/pi;
%Remat(n,:) = [Re_ta Re_de];
n = n+1;

end

% Pull experimental stuff
exp_the_res

% Plot the convection coefficients
figure(1)
plot(wemat,hdmat,'k-',wemat,htamat,'k--')
xlabel('Angular Velocity \omega (rad/s)')
ylabel('Convection Coefficient h (W/m^2-K)')
legend('Dean Flow','Couette/Taylor-Couette Flow','Location','Best')

% Plot the experimental thermal resistance and the full correlation
figure(2)
scatter(wmat,Rth_ex,'k')
axis([0 700 0 20])
hold on
%lsline
plot(Tamat,rthmat,'k')
%plot(Tamat,rthmat2,'k--')
legend('Experiment','Full','Dean','Location','Best')
xlabel('Angular Velocity \omega (rpm)')
ylabel('Thermal Resistance (K/W)')

% Plot the thermal resistances and the 95% confidence lines and the
% uncertainty bands
figure(3)
scatter(wmat,Rth_ex,'k')
axis([250 700 0 20])
hold on
%lsline
plot(Tamat,rthmat,'k.')
plot(Tamat,rthmat2,'k')
plot(Tamat,urthup,'k-.')
```

```
plot(Tamat,urthdn,'k-.')
plot(Tamat,urthup2,'k--')
plot(Tamat,urthdn2,'k--')
legend('Experiment','Full Correlation','Dean
Correlation','Location','Best')
xlabel('Angular Velocity \omega (rpm)')
ylabel('Thermal Resistance (K/W)')

%figure(4)
errorbar(wmat,Rth_ex,1.96*urth,'ok')
axis([250 700 8 20])
```

Experimental Data Uncertainty

```
% Experimental thermal resistance
% Program: exp_the_res_2

% This code will just be where we calculate the thermal resistance and
% uncertainty for the experimental part of the project.

% clear all; close all; clc

dex = 1;        % Counting variable
ub = 1;         % Systematic uncertainty of temperature

utime = 1/60;       % Error on time, s
time = 20;          % Time videos were taken over
prw = 0.5;          % Error on angular velocity, rev

heatr = 38.8;       % Heater power

n = 300;

% Begin experimental runs. The following description shows what each
set of
% values is

% Test run number
% Test file
% Heat flow through bearing
% Systematic uncertainty for temperature
% Total uncertainty for temperature
% Voltage uncertainty
% Temperature uncertainty
% Total heater power uncertainty
% Thermal resistance of the bearing for the test run
% Uncertainty of the thermal resistance for the test run
% Angular velocity set used to calcualte the angular velocity
% Total angular velocity uncertainty
% Temperature value of the run to be stored in the matrix
% Advance the counter

%1
Oct6_11_run1
qmat(dex) = q;
```

```
anov(:,1) = deltaT(344:344+n);
up = sqrt((stdev/sqrt(size(deltaT,1)))^2+0.5^2);
utt(dex) = sqrt(up^2+ub^2)/aver;
uv = sqrt(0.051^2+(0.005*batt+0.01)^2);
ur = sqrt(0.05^2+(0.008*heatr+0.04)^2);
uqq(dex) = sqrt(4*(uv/batt)^2+(ur/heatr)^2);
Rth_ex(dex) = aver/q;
urth(dex) = sqrt(2*utt(dex)^2+uqq(dex)^2);
w3 = w/3;
uww(dex) = sqrt((prw/w3)^2 + (utime/time)^2);
wmat(dex) = w;
memat(dex) = aver;
dex = dex+1;

%2
Oct7_11_run1
qmat(dex) = q;
anov(:,2)=deltaT(333:333+n);
up = sqrt((stdev/sqrt(size(deltaT,1)))^2+0.5^2);
utt(dex) = sqrt(up^2+ub^2)/aver;
uv = sqrt(0.051^2+(0.005*batt+0.01)^2);
ur = sqrt(0.05^2+(0.008*heatr+0.04)^2);
uqq(dex) = sqrt(4*(uv/batt)^2+(ur/heatr)^2);
Rth_ex(dex) = aver/q;
urth(dex) = sqrt(2*utt(dex)^2+uqq(dex)^2);
w3 = w/3;
uww(dex) = sqrt((prw/w3)^2 + (utime/time)^2);
wmat(dex) = w;
memat(dex) = aver;
dex = dex+1;

%3
Oct10_11_run1
qmat(dex) = q;
anov(:,3) = deltaT(437:437+n);
up = sqrt((stdev/sqrt(size(deltaT,1)))^2+0.5^2);
utt(dex) = sqrt(up^2+ub^2)/aver;
uv = sqrt(0.051^2+(0.005*batt+0.01)^2);
ur = sqrt(0.05^2+(0.008*heatr+0.04)^2);
uqq(dex) = sqrt(4*(uv/batt)^2+(ur/heatr)^2);
Rth_ex(dex) = aver/q;
urth(dex) = sqrt(2*utt(dex)^2+uqq(dex)^2);
w3 = w/3;
uww(dex) = sqrt((prw/w3)^2 + (utime/time)^2);
wmat(dex) = w;
memat(dex) = aver;
dex = dex+1;

%4
Oct10_11_run2
qmat(dex) = q;
anov(:,4) = deltaT(288:288+n);
up = sqrt((stdev/sqrt(size(deltaT,1)))^2+0.5^2);
utt(dex) = sqrt(up^2+ub^2)/aver;
uv = sqrt(0.051^2+(0.005*batt+0.01)^2);
```

```
ur = sqrt(0.05^2+(0.008*heatr+0.04)^2);
uqq(dex) = sqrt(4*(uv/batt)^2+(ur/heatr)^2);
Rth_ex(dex) = aver/q;
urth(dex) = sqrt(2*utt(dex)^2+uqq(dex)^2);
w3 = w/3;
uww(dex) = sqrt((prw/w3)^2 + (utime/time)^2);
wmat(dex) = w;
memat(dex) = aver;
dex = dex+1;

%5
Oct10_11_run3
qmat(dex) = q;
anov(:,5) = deltaT(334:334+n);
up = sqrt((stdev/sqrt(size(deltaT,1)))^2+0.5^2);
utt(dex) = sqrt(up^2+ub^2)/aver;
uv = sqrt(0.051^2+(0.005*batt+0.01)^2);
ur = sqrt(0.05^2+(0.008*heatr+0.04)^2);
uqq(dex) = sqrt(4*(uv/batt)^2+(ur/heatr)^2);
Rth_ex(dex) = aver/q;
urth(dex) = sqrt(2*utt(dex)^2+uqq(dex)^2);
w3 = w/3;
uww(dex) = sqrt((prw/w3)^2 + (utime/time)^2);
wmat(dex) = w;
memat(dex) = aver;
dex = dex+1;

%6
Oct10_11_run4
qmat(dex) = q;
anov(:,6) = deltaT(188:188+n);
up = sqrt((stdev/sqrt(size(deltaT,1)))^2+0.5^2);
utt(dex) = sqrt(up^2+ub^2)/aver;
uv = sqrt(0.051^2+(0.005*batt+0.01)^2);
ur = sqrt(0.05^2+(0.008*heatr+0.04)^2);
uqq(dex) = sqrt(4*(uv/batt)^2+(ur/heatr)^2);
Rth_ex(dex) = aver/q;
urth(dex) = sqrt(2*utt(dex)^2+uqq(dex)^2);
w3 = w/3;
uww(dex) = sqrt((prw/w3)^2 + (utime/time)^2);
wmat(dex) = w;
memat(dex) = aver;
dex = dex+1;

%7
Oct14_11_run1
qmat(dex) = q;
anov(:,7) = deltaT(302:302+n);
up = sqrt((stdev/sqrt(size(deltaT,1)))^2+0.5^2);
utt(dex) = sqrt(up^2+ub^2)/aver;
uv = sqrt(0.051^2+(0.005*batt+0.01)^2);
ur = sqrt(0.05^2+(0.008*heatr+0.04)^2);
uqq(dex) = sqrt(4*(uv/batt)^2+(ur/heatr)^2);
w3 = w/3;
uww(dex) = sqrt((prw/w3)^2 + (utime/time)^2);
```

```
Rth_ex(dex) = aver/q;
urth(dex) = sqrt(2*utt(dex)^2+uqq(dex)^2);
wmat(dex) = w;
memat(dex) = aver;
dex = dex+1;

%8
Oct14_11_run2
qmat(dex) = q;
anov(:,8) = deltaT(527:527+n);
up = sqrt((stdev/sqrt(size(deltaT,1)))^2+0.5^2);
utt(dex) = sqrt(up^2+ub^2)/aver;
uv = sqrt(0.051^2+(0.005*batt+0.01)^2);
ur = sqrt(0.05^2+(0.008*heatr+0.04)^2);
uqq(dex) = sqrt(4*(uv/batt)^2+(ur/heatr)^2);
Rth_ex(dex) = aver/q;
urth(dex) = sqrt(2*utt(dex)^2+uqq(dex)^2);
w3 = w/3;
uww(dex) = sqrt((0)^2 + (utime/time)^2);
wmat(dex) = w;
memat(dex) = aver;
dex = dex+1;

%9
Oct14_11_run3
qmat(dex) = q;
anov(:,9) = deltaT(410:410+n);
up = sqrt((stdev/sqrt(size(deltaT,1)))^2+0.5^2);
utt(dex) = sqrt(up^2+ub^2)/aver;
uv = sqrt(0.051^2+(0.005*batt+0.01)^2);
ur = sqrt(0.05^2+(0.008*heatr+0.04)^2);
uqq(dex) = sqrt(4*(uv/batt)^2+(ur/heatr)^2);
Rth_ex(dex) = aver/q;
urth(dex) = sqrt(2*utt(dex)^2+uqq(dex)^2);
w3 = w/3;
uww(dex) = sqrt((prw/w3)^2 + (utime/time)^2);
wmat(dex) = w;
memat(dex) = aver;
dex = dex+1;

%10
Oct17_11_run1
qmat(dex) = q;
anov(:,10) = deltaT(401:401+n);
up = sqrt((stdev/sqrt(size(deltaT,1)))^2+0.5^2);
utt(dex) = sqrt(up^2+ub^2)/aver;
uv = sqrt(0.051^2+(0.005*batt+0.01)^2);
ur = sqrt(0.05^2+(0.008*heatr+0.04)^2);
uqq(dex) = sqrt(4*(uv/batt)^2+(ur/heatr)^2);
Rth_ex(dex) = aver/q;
urth(dex) = sqrt(2*utt(dex)^2+uqq(dex)^2);
w3 = w/3;
uww(dex) = sqrt((prw/w3)^2 + (utime/time)^2);
wmat(dex) = w;
memat(dex) = aver;
```

```
dex = dex+1;

%11
Oct17_11_run2
qmat(dex) = q;
anov(:,11) = deltaT(310:310+n);
up = sqrt((stdev/sqrt(size(deltaT,1)))^2+0.5^2);
utt(dex) = sqrt(up^2+ub^2)/aver;
uv = sqrt(0.051^2+(0.005*batt+0.01)^2);
ur = sqrt(0.05^2+(0.008*heatr+0.04)^2);
uqq(dex) = sqrt(4*(uv/batt)^2+(ur/heatr)^2);
Rth_ex(dex) = aver/q;
urth(dex) = sqrt(2*utt(dex)^2+uqq(dex)^2);
w3 = w/3;
uww(dex) = sqrt((prw/w3)^2 + (utime/time)^2);
wmat(dex) = w;
memat(dex) = aver;
dex = dex+1;

%12
Oct17_11_run3
qmat(dex) = q;
anov(:,12) = deltaT(229:229+n);
up = sqrt((stdev/sqrt(size(deltaT,1)))^2+0.5^2);
utt(dex) = sqrt(up^2+ub^2)/aver;
uv = sqrt(0.051^2+(0.005*batt+0.01)^2);
ur = sqrt(0.05^2+(0.008*heatr+0.04)^2);
uqq(dex) = sqrt(4*(uv/batt)^2+(ur/heatr)^2);
Rth_ex(dex) = aver/q;
urth(dex) = sqrt(2*utt(dex)^2+uqq(dex)^2);
w3 = w/3;
uww(dex) = sqrt((prw/w3)^2 + (utime/time)^2);
wmat(dex) = w;
memat(dex) = aver;
dex = dex+1;

%13
Oct17_11_run4
qmat(dex) = q;
anov(:,13) = deltaT(300:300+n);
up = sqrt((stdev/sqrt(size(deltaT,1)))^2+0.5^2);
utt(dex) = sqrt(up^2+ub^2)/aver;
uv = sqrt(0.051^2+(0.005*batt+0.01)^2);
ur = sqrt(0.05^2+(0.008*heatr+0.04)^2);
uqq(dex) = sqrt(4*(uv/batt)^2+(ur/heatr)^2);
Rth_ex(dex) = aver/q;
urth(dex) = sqrt(2*utt(dex)^2+uqq(dex)^2);
w3 = w/3;
uww(dex) = sqrt((prw/w3)^2 + (utime/time)^2);
wmat(dex) = w;
memat(dex) = aver;
dex = dex+1;

%14
Oct17_11_run6
```

```
qmat(dex) = q;
anov(:,14) = deltaT(210:210+n);
up = sqrt((stdev/sqrt(size(deltaT,1)))^2+0.5^2);
utt(dex) = sqrt(up^2+ub^2)/aver;
uv = sqrt(0.051^2+(0.005*batt+0.01)^2);
ur = sqrt(0.05^2+(0.008*heatr+0.04)^2);
uqq(dex) = sqrt(4*(uv/batt)^2+(ur/heatr)^2);
Rth_ex(dex) = aver/q;
urth(dex) = sqrt(2*utt(dex)^2+uqq(dex)^2);
w3 = w/3;
uww(dex) = sqrt((prw/w3)^2 + (utime/time)^2);
wmat(dex) = w;
memat(dex) = aver;
dex = dex+1;

%15
Oct18_11_run1
qmat(dex) = q;
anov(:,15) = deltaT(285:285+n);
up = sqrt((stdev/sqrt(size(deltaT,1)))^2+0.5^2);
utt(dex) = sqrt(up^2+ub^2)/aver;
uv = sqrt(0.051^2+(0.005*batt+0.01)^2);
ur = sqrt(0.05^2+(0.008*heatr+0.04)^2);
uqq(dex) = sqrt(4*(uv/batt)^2+(ur/heatr)^2);
Rth_ex(dex) = aver/q;
urth(dex) = sqrt(2*utt(dex)^2+uqq(dex)^2);
w3 = w/3;
uww(dex) = sqrt((0)^2 + (utime/time)^2);
wmat(dex) = w;
memat(dex) = aver;

% This next section will caluclate the thermal resistance for the
straight
% shaft.

w_shaft = [432
468
561
587
555
438
345
366
329
417
471
509];

bat_begin = [8.82
8.14
7.88
7.66
7.34
7.33
7.17
```

```
7.38
6.85
6.84
8.85
8.18];

bat_end = [7.83
7.55
7.3
7.06
6.89
6.73
6.61
6.53
6.34
5.95
7.89
7.55];

bat_ave = ((bat_begin+bat_end)/2 + bat_end)/2;

dt_shaft = [18
17
16
11
19
15
14
14
12
11
18
18];

q_shaft = bat_ave.^2/heatr;

Rth_shaft = dt_shaft./q_shaft;

figure(4)
scatter(wmat,Rth_ex,'kd')
hold on
scatter(w_shaft,Rth_shaft,'k')
xlabel('Angular Velocity (rpm)')
ylabel('Thermal Resistance (K/W)')
axis([250 600 0 17])
legend('Uncorrected Bearing Thermal Resistance',...
    'Uncorrected Shaft Thermal Resistance','Location','Best')

mshaft = mean(Rth_shaft);
qsplit = mshaft./(Rth_ex+mshaft).*qmat;
Rth_ex_1 = mean(anov)./qsplit;


mexp = mean(Rth_ex);
```

```
% Uncertainty on shaft percentage
t1=((Rth_ex*mshaft)./(Rth_ex*mshaft)).^2*(uqq/qmat)^2;
t2 = (qmat.*((Rth_ex+mshaft)*mshaft-mshaft*Rth_ex)/
(mshaft+Rth_ex).^2)^2*urth.^2;
t3 = ((qmat.*((Rth_ex+mshaft).*Rth_ex-mshaft*Rth_ex)./
(mshaft+Rth_ex).^2).^2).*(urth.^2);
perc = sqrt(t1.^2+t2.^2+t3.^2);
```

Taylor Section Nusselt Number Calculation Function

```
function unta = utafun(Ta, Pr, Gr, unu, Nuc, utata, ug, uprpr)


% This function will calculate the uncertainty of the Taylor section
% Nusselt number.

unta = sqrt(((Ta/1708)^((Pr/Gr)^(1/6)/2))^2*unu^2 + ((Nuc*(Ta/1708)^...
    ((Pr/Gr)^(1/6)/2-1)*(Pr/Gr)^(1/6))/3416)^2*(utata*Ta)^2 +
(Nuc*(Ta/...
    1708)^((Pr/Gr)^(1/6)/2)*log(Ta/1708)/(12*Gr^2*(Pr/Gr)^(5/6)))^2*...
    ug^2 + (Nuc*(Ta/1708)^((Pr/Gr)^(1/6)/2)*log(Ta/1708)/
(12*Gr*(Pr/Gr)^...
    (5/6)))^2*(uprpr*Pr)^2);
```

Dean Section Nusselt Number Calculation Function

```
function [ux1 ux2 unude] = udeanfun(De, Pr, udede, uprpr, x1, x2)

ux1 = sqrt(4*(957/(De^3*Pr))^2*(udede*De)^2+(957/
(De^2*Pr^2))^2*(uprpr*...
    Pr)^2);
ux2 = sqrt((0.477/Pr^2)^2*(uprpr*Pr)^2);
unude = sqrt((4.343*(4.343/x1+3.657)^2/
(x1^2*((4.343/x1+3.657)^3+1.158*...
    (De/x2)^3/2)^(2/3)))^2*ux1^2 + (0.579*De*sqrt(De/x2)/
(x2^2*((4.343/...
    x1+3.657)^3+1.158*(De/x2)^3/2)^(2/3)))^2*ux2^2 +
(0.579*sqrt(De/x2)/...
    (x2*((4.343/x1+3.657)^3+1.158*(De/x2)^3/2)^(2/3)))^2*ux2^2);
```